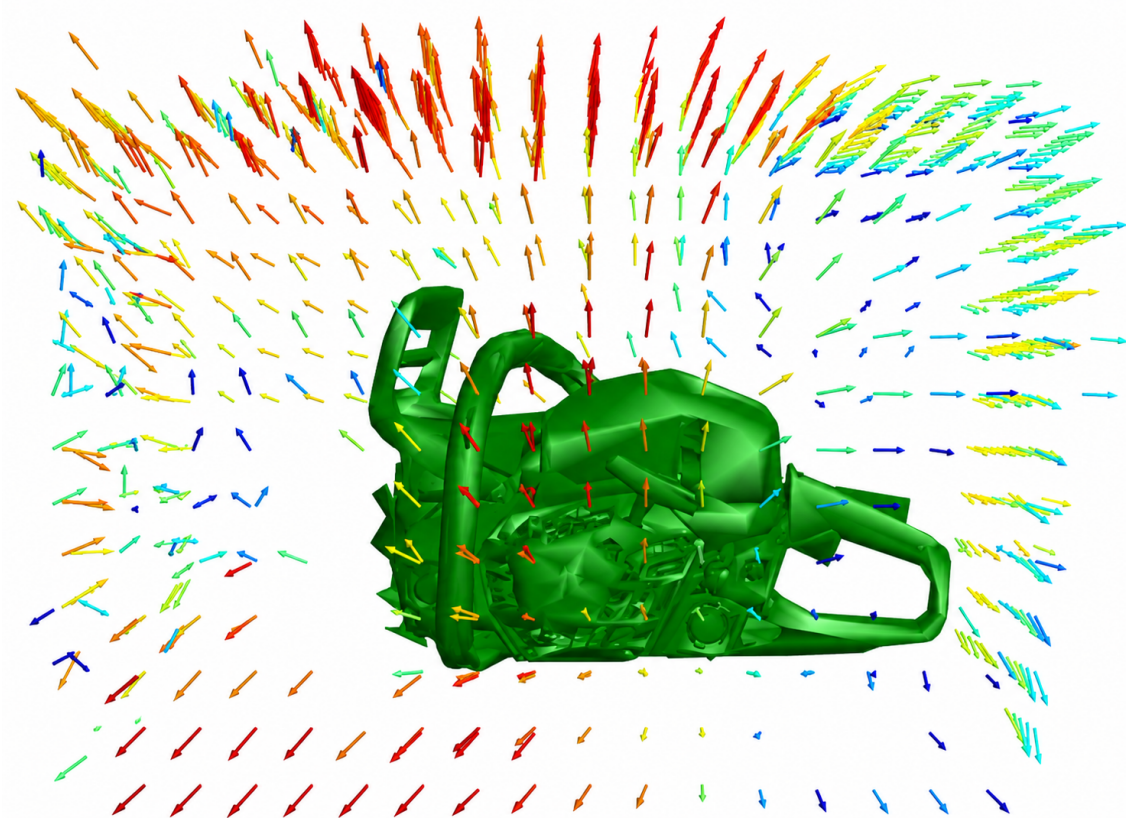


Investigation of Intake Sound Reduction on Chainsaws

Master's thesis in the Master's Programme Sound and Vibration, at the Division of Applied Acoustics

Shko Mirza

DEPARTMENT OF ARCHITECTURE AND CIVIL ENGINEERING
CHALMERS UNIVERSITY OF TECHNOLOGY
Gothenburg, Sweden 2026
www.chalmers.se

MASTER'S THESIS 2026

Investigation of Intake Sound Reduction on Chainsaws

Shko Mirza



CHALMERS
UNIVERSITY OF TECHNOLOGY

Department of Architecture and Civil Engineering
Division of Applied Acoustic
Chalmers University of Technology
Gothenburg, Sweden 2026

Investigation of Intake Sound Reduction on Chainsaws
Shko Mirza

© Shko Mirza, 2026.

Supervisor: Fredrik Wibling, Husqvarnagroup Physical & Durability Lab
Supervisor: Krister Larsson, Chalmers University of Technology
Examiner: Astrid Pieringer, Chalmers University of Technology

Master's Thesis 2026
Department of Architecture and Civil Engineering
Chalmers University of Technology
SE-412 96 Gothenburg
Sweden
Telephone +46 31 772 1000

Cover: Measured active intensity, A weighted, at fourth engine order using scan and paint.

Typeset in LaTeX
Gothenburg, Sweden 2026

Investigation of Intake Sound Reduction on Chainsaws
SHKO MIRZA
Department of Architecture and Civil Engineering
Chalmers University of Technology

Abstract

Chainsaws generate high noise levels that pose risks to both operators and the surrounding environment. As regulatory noise limits for outdoor equipment tighten, noise reduction is of growing importance. Since even basic exhaust silencers can leave the intake side as the dominant noise source, exhaust side improvements alone are insufficient to meet stricter requirements. This makes intake noise reduction an increasingly relevant area of development. This thesis investigates acoustic noise reduction measures for the intake system of a Husqvarna two-stroke chainsaw engine, with the aim of reducing radiated sound power without compromising engine performance or requiring major modifications to the existing chassis geometry.

The study followed a three-stage simulation approach using COMSOL Multiphysics, progressing from simplified cylindrical duct models to increasingly realistic intake geometries. Quarter-wave tube (QWT) resonators, Helmholtz resonators (HHR), hybrid resonator configurations, and muffler designs were evaluated through simulated transmission loss and insertion loss. The fourth engine order at 680 Hz was identified as the dominant intake noise frequency and became the primary design target. Based on simulation results and practical constraints of space and manufacturability, QWT resonators were selected as the most feasible design concept and prototyped using 3D printing for experimental validation.

Experimental measurements confirmed that resonator placement has a significant effect on attenuation performance. Positioning the resonator adjacent to the cylinder, yielded substantially greater insertion loss than placement near the outlet. It was found that a single front-mounted QWT achieves comparable attenuation to four resonators mounted at the rear of the duct. Bending the resonator to fit within the chainsaw chassis introduced a downward shift in resonance frequency but did not reduce attenuation effectiveness. The simulated models consistently overpredicted attenuation amplitude compared to measurements, largely due to the absence of damping and simplified geometry. When damping was incorporated into the simulation model, agreement with experimental results improved considerably. The study concludes that QWT resonators are a viable approach to intake noise reduction in compact two-stroke engines, provided that the geometry of the chainsaw can't be altered.

Keywords: Chainsaw, Two-stroke engine, Intake, Quarter wave tube, Helmholtz resonator, Muffler, COMSOL, Engine order.

Acknowledgements

This thesis was carried out in collaboration with Husqvarna, specifically within the Physical & Durability Lab. I would like to begin by expressing my sincere gratitude to my supervisor Fredrik Wibling and Filip Stenlund for their guidance, support, and the trust they had in me throughout this process. I would also like to extend my thanks to the rest of the team at the division, you made my time unforgettable.

To my academic supervisor Krister Larsson, thank you for always making time for me and for continuously broadening my understanding of the subject. I would also like to thank my examiner Astrid Pieringer for her attentiveness and for consistently checking in on my progress throughout the work.

I am grateful to the team at Brekke & Strand for generously allowing me to use their facilities during the writing of this thesis.

A special thanks to my peers in the Matser's program who continuously pushed me to work harder, our time at the division is something that will stay with me forever.

Finally, and most deeply, my gratitude goes to my family. Your unconditional love and support has been the foundation of everything I have accomplished, and none of this would have been possible without you!

Shko Mirza, Gothenburg, June 2026

AI disclosure

In this study, Claude AI has been used as a language aid tool to improve grammar and phrasing, create tables in LaTeX format, and assist in the literature search. No AI tools were used to generate design proposals, COMSOL modeling, or MATLAB data processing and analysis.

List of Acronyms

Below is the list of acronyms that have been used throughout this thesis listed in alphabetical order:

EI	Enviromental impact
HHR	Helmholtz resonator
IL	Insertion loss
ODELIA	Outdoor equipment limit assessment
QWT	Quarter wave tube
SPL	Sound pressure level
TL	Transmission loss

Nomenclature

Below is the nomenclature of indices, sets, parameters, and variables that have been used throughout this thesis.

Indices

m	Number of pressure nodal diameters in a duct cross section
n	Number of pressure nodal circles in a duct cross section

Parameters

c	Speed of sound [m/s]
c_0	Speed of sound at reference conditions [m/s]
γ	Ratio of specific heats for air (=1.4) [-]
R	Molar universal gas constant (=8.314) [J $\text{mol}^{-1}\text{K}^{-1}$]
M	Average molar mass of air (=0.02857) [kg mol^{-1}]
M_a	Mach number [-]
ρ_0	Ambient air density [kg/m^3]
σ	Flow resistivity of porous material [$\text{Pa} \cdot \text{s/m}^2$]
σ_p	Area porosity [-]
$\alpha_{m.n}$	Transverse wavenumber $\times$ duct radius for mode (m, n) [-]
D	Duct diameter [m]
L	length of duct or cavity [m]
L_{eff}	Effective length of QWT including end correction [m]
l_c	chamber or neck length [m]
l_h	Neck length of Helmholtz resonator [m]
r	Duct or resonator radius [m]
b	Hole radius of Helmholtz resonator [m]

S	Cross sectional area of resonator opening [m^2]
V	Cavity volume of resonator [m^3]
V_d	Engine displacement [cc]
m	Expansion ratio of muffler, S_2/S_1 [-]

Variables

f	Frequency [Hz]
f_{QWT}	Resonance frequency of quarter wave tube [Hz]
f_0	Target resonance frequency [Hz]
f_c	Cutoff frequency of a duct mode [Hz]
k	wavenumber [rad/m]
T	Gas temperature [K]
p	Acoustic pressure [Pa]
W_i	Incident sound power [W]
W_t	Transmitted sound power [W]
W_1	Radiated sound power before silencer implementation [W]
W_1	Radiated sound power after silencer implementation [W]
L_{W1}	Sound power level before silencer installation [dB]
L_{W2}	Sound power level after silencer installation [dB]
L_{peq}	Equivalent sound pressure level at operator position [dB(A)]

Contents

List of Acronyms x

Nomenclature xiii

List of Figures xvii

1 Introduction 1
- 1.1 Background . . . 1
- 1.2 Aim & Objective . . . 3
- 1.3 Research questions . . . 3
- 1.4 Limitations . . . 3

2 Theory 5
- 2.1 Fundamental operation of a simple two-stroke engine . . . 5
- 2.2 Noise sources in a simple two-stroke engine . . . 6
- 2.3 Side branch Resonators . . . 7
  - 2.3.1 Helmholtz resonator . . . 7
  - 2.3.2 Quarter wave tube resonator . . . 8
  - 2.3.3 Combining the QWT and the Helmholtz resonator . . . 9
- 2.4 Muffler . . . 10
- 2.5 Plane Wave Propagation . . . 12
  - 2.5.1 Higher Order Modes . . . 12
  - 2.5.2 Cutoff frequency . . . 13
  - 2.5.3 Effect of Mean Flow . . . 13
- 2.6 Transmission Loss in ducts . . . 14
- 2.7 Insertion loss . . . 14
- 2.8 Technical Framework . . . 14

3 Methods 17
- 3.1 Baseline acoustic profile . . . 17
- 3.2 Initial Simulations . . . 18
  - 3.2.1 Quarter wave tube . . . 19
  - 3.2.2 Helmholtz resonator . . . 21
  - 3.2.3 Combining the quarter wave tube and Helmholtz resonator . . . 22
  - 3.2.4 Optimizing the placement . . . 22
  - 3.2.5 Muffler . . . 23
- 3.3 Intermediate simulation stage . . . 25

3.3.1 Design proposals . . . 25
3.3.2 Simulated IL . . . 26
3.4 Detailed simulation stage . . . 28
3.4.1 Detailed design proposal . . . 29
3.4.2 System excitation . . . 30
3.4.3 Detailed stage Simulated IL . . . 30
3.5 Tuning/ Troubleshooting the detailed model . . . 31
3.6 Validating the design proposals . . . 32
3.7 Design process . . . 33

4 Results **35**
4.1 Intermediate stage design proposals . . . 35
4.1.1 Crank house measurements . . . 35
4.1.1.1 Insertion loss resonator . . . 35
4.1.1.2 Insertion loss muffler . . . 36
4.1.2 Intake duct measurements . . . 37
4.1.2.1 Insertion loss resonator . . . 37
4.1.2.2 Insertion loss Muffler . . . 38
4.2 Detailed model loudspeaker measurements . . . 38
4.2.1 Crank house measurements . . . 38
4.2.2 Inlet duct measurements . . . 40
4.3 Experimental tuning design solution . . . 42
4.3.1 Resonator placement . . . 42
4.3.2 Number of resonators . . . 43
4.3.3 Bending the resonator . . . 43
4.3.4 Piped and coned outlet . . . 45
4.4 Tuning of the simulation model . . . 45

5 Discussion **47**
5.1 Including engine body simulations . . . 47
5.2 Amplitude difference between simulations and measurements . . . 48
5.3 Duct to Resonator Surface Area Ratio . . . 48
5.4 Resonator placement and pressure antinodes . . . 49
5.5 Bending the resonator . . . 49
5.6 Production inefficiencies . . . 50

6 Conclusion **51**
6.1 Future work . . . 52

Bibliography **53**

List of Figures

2.1 Operational stages and principal components of the two-stroke engine cycle [1, p. 6]. Reprinted with permission. 5
2.2 Various noise sources radiating from a two-stroke engine [1, p. 546]. Reprinted with permission. 7
2.3 Configuration of a Helmholtz resonator 7
2.4 Configuration of a QWT 8
2.5 Simple expansion chamber 10
2.6 Theoretical effect of expansion ratio,m, and chamber length,l_c, on the attenuation. 11
2.7 Absorptive muffler 12
2.8 Microphone positions on hemisphere, A is the reference box, d0 is the characteristic source dimension, r is the hemisphere radius $\geq$ 2d0 [2, p. 3]. Reprinted with permission. 14

3.1 Average A-weighted SPL emitted from the chainsaw, measured in accordance with ISO 22868:2021 [2]. The blue line shows the average SPL including the exhaust contribution, the red line shows the average SPL with a heavily silenced exhaust pipe. By courtesy of Fredrik Wibling. 17
3.2 QWT coupled to main duct 19
3.3 Schematic of the three QWT geometries evaluated: straight (left), 90° bend with 15 mm bend radius (centre), and sharp 90° bend (right). 19
3.4 Transmission loss for three QWT with different angles of bending, 0, 15, 90 degrees 20
3.5 Simulated TL for QWT with different resonator opening surface areas in comparison to main duct surface area 20
3.6 TL curve for Helmholtz resonator initial simulations 21
3.7 Comparison of simulated TL for three different resonator types, QWT, Helmholtz resonator and a combination of the two. 22
3.8 Resonator placed on different positions, close to the incident port, in the middle of the duct and lastly at the end of the simplified intake duct where the acoustic wave leaves 22
3.9 Transmission loss of a resonator depending on placement along main duct in x direction. 23
3.10 Simple expansion chamber modeled in COMSOL. 24
3.11 Simulated TL for each muffler configuration. 24

3.12 Intake port geometry used for intermediate simulations stage 25
3.13 Intermediate design proposals of noise reduction measures on main pipe. 26
3.14 Simulated IL for the design proposals suggested in the intermediate simulation stage including and excluding the body of the cone which the upstream signal comes from. 27
3.15 Intake port geometry used for detailed simulation stage 29
3.16 Simulated IL from the detailed design stage. The plot compares the IL resulting from pressure-based versus velocity-based excitation at the incident port for each design proposal (QWTs and their corresponding resonance frequencies). 31
3.17 Measurement setup schematics 32
3.18 Measurement setup 33
3.19 Flowchart illustrating the design and validation process for an intake noise reduction component. 34

4.1 Measured and simulated IL for resonator coupled to main duct 36
4.2 Measured and simulated Insertion Loss (IL) for the perforated duct muffler with an empty cavity versus a cavity filled with porous material. 36
4.3 Measured and simulated IL for the resonator coupled to the main duct 37
4.4 Measured and simulated IL for the muffler configurations 38
4.5 Measured and simulated IL for each detailed design proposal. Measurement conducted using Loudspeaker sending signal through crank house through to the intake duct. Signal measured 5 Cm away from intake duct. 39
4.6 Measured and simulated IL. Measurement conducted using Loudspeaker sending signal through cone to the intake duct. Signal measured 5cm away from intake duct. 41
4.7 Measured Resonator placement 42
4.8 Comparing IL of intake pipe with different amount of QWT coupled to the system 43
4.9 Comparison of one QWT in the front and 4 QWT in the back 44
4.10 Bent QWT compared to straight QWT 44
4.11 Comparison of Piped outlet and straight outlet 45
4.12 Measured IL for front mounted QWT and simulated IL, including damping in simulation model 46
4.13 Measured IL for one front mounted QWT with simulated IL for one and three front mounted QWT including damping in simulation model. 46

1

Introduction

1.1 Background

Chainsaws generate high noise levels, which can negatively affect both the operator's hearing and the surrounding environment. Over the past decade, the market for equipment has developed in many terms, including the demand for quieter equipment. Directive 2000/14/EC is a part of the European Union strategy to reduce noise at source, in particular noise emissions from outdoor equipments. Since the limits have remained unchanged for many years, there is a need to revise existing limits and, where justified, introduce new limits for equipment not yet regulated. The ODELIA study (**O**ut**D**oor **E**quipment **LI**mit **A**ssessment),a study for the European commission, conducted by TNO addressed this need [3].

The environmental impact (EI) indicator is a composite ranking metric that accounts for the following factors across the whole EU [3]:

- The average guaranteed sound power level, used as a representative value for typical operating conditions.
- The number of machines in service within each characteristic area of usage.
- The duration and patterns of usage.
- Penalty weights applied for noise that is tonal, impulsive, or fluctuating in character, as well as for equipment operated during night-time hours.
- The number of people exposed to the noise in each type of environment, such as urban, suburban, residential, and rural settings.

A wide range of outdoor equipment was assessed with the EI indicator, and the ratings are shown in Table 1.1. The criterion for changing or introducing limits is between low or medium, so EI $\geq$ 47 dB , but if EI is just below 47 dB it may give rise to discussion [3].

The ODELIA study showed that the EI value for a portable chainsaw equipped with a combustion engine is around 67 dB, indicating a very high EI rating. Thus the study proposed a noise limit for the chainsaw, which currently has none. The limit proposed for a chainsaw equipped with a combustion engine was 111 + 2P dB, where P is the engine power expressed in kW [3].

Rating	Range of environmental impact indicator EI in dB
Very low	< 37
Low	37–46
Medium	47–56
High	57–67
Very high	> 67

Table 1.1: Environmental impact indicator ratings from the ODELIA study [3].

On the American market there is set criteria which states that the equivalent sound pressure level (SPL) at the ear of the operator shall not exceed the following limit [4]:

$$L_{\text{peq(max)}} = 0.16\, V_d + 97, \quad \text{or} \quad L_{\text{peq(max)}} = 108 \text{ dB(A)}.$$

Where V_d is the displacement of the engine given in cc.

The value which is less of the two should be applied, and measurements are to be carried out in accordance with ISO 22868:2021. Same criteria is applied for the Canadian market[5]. Therefore working with noise emitted from chainsaws has become more relevant and important.

Typically the exhaust system of a two-stroke engine is considered the dominant noise source, however, improvements in exhaust silencing may shift the relative contribution of the intake system, making it a significant contributor to the total sound power level [1].

The intake process is governed by rapid pressure fluctuations caused by the cyclic opening and closing of the intake port and the piston motion. These periodic induction events generate strong pressure pulses that propagate through the intake duct[1, p.546]. As a result, the intake noise contains both tonal components, related to engine firing frequency and its harmonics, and broadband components generated by turbulent flow[6].

Furthermore, the intake system is directly coupled to engine performance. Any modification to the intake duct geometry may influence its performance [7]. Therefore, acoustic improvements must be achieved without compromising engine power output, or fuel efficiency.

Another complicating factor is the limited available space and strict constraints on weight in handheld machinery such as chainsaws. To keep the design compact and lightweight, all solutions require small dimension to preserve the power-to-weight ratio and ergonomic usability.

For these reasons, intake noise reduction in two-stroke engines represents a multidisciplinary challenge involving acoustics, fluid dynamics and mechanical design. A systematic investigation is therefore required to characterize the intake sound field and evaluate feasible noise reduction concepts under realistic operating conditions.

1.2 Aim & Objective

The aim of this thesis is to investigate the intake-related sound power levels of Husqvarna chainsaws equipped with two-stroke engines, and to identify, develop, and evaluate solutions for reducing the total sound power emitted from the inlet system.

To achieve this aim, the work of the thesis adheres to the following objectives:

- Conduct a literature study on the operating principles of two-stroke engines.
- Conduct a literature study on general duct acoustics and sound attenuation methods and examine their applicability to the inlet systems of two-stroke engines.
- Gain an understanding of the design and operation of Husqvarna chainsaws.
- Propose design solutions to reduce intake related sound emissions in Husqvarna chainsaws.
- Evaluate the acoustic attenuation performance of the proposed solutions relative to the baseline configuration.

1.3 Research questions

To fulfill the aims and objectives the thesis addresses the following research questions:

- How can the intake port be optimized to reduce the sound power level while maintaining engine performance as much as possible?
- Which design parameters have the most significant influence on the radiated sound power level?
- Does the proposed design result in a measurable reduction in sound power level?

1.4 Limitations

The following limitations apply to this study:

- The scope is limited to intake related sound emissions of the two-stroke engine. Noise generated by other engine components or mechanical parts of the chainsaw falls outside the scope of this study.
- Although the study would benefit from coupled flow and fluid simulations, time constraints limit the analysis to pressure acoustic simulations only.
- No modifications to the existing chainsaw chassis or overall geometry are permitted. All intake design proposals must be compatible with the surrounding

chainsaw components.

- All design proposals are designed with full-load engine operating conditions as the basis for dimensioning, such as exhaust and intake temperature, and dominant engine orders.

2

Theory

2.1 Fundamental operation of a simple two-stroke engine

To get an understanding for the sound radiated from the intake port of the two-stroke engine, a fundamental understanding of the complete engine must be established.

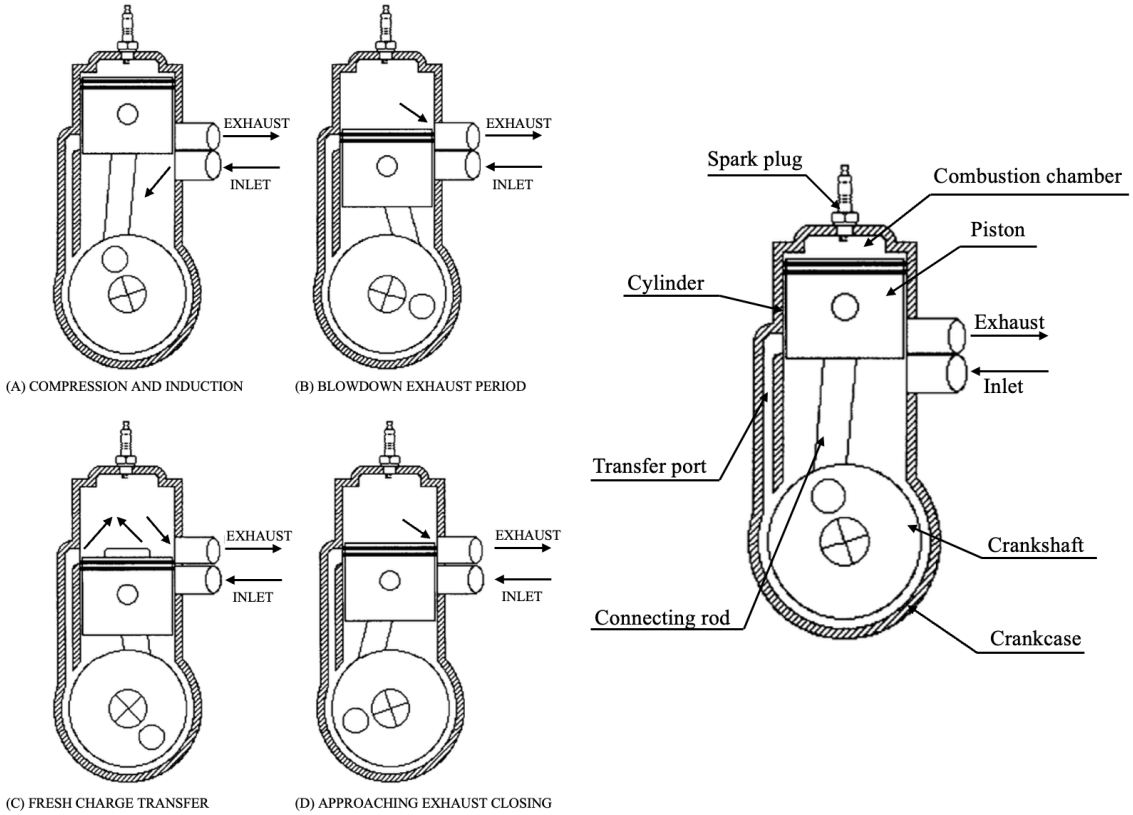


Figure 2.1: Operational stages and principal components of the two-stroke engine cycle [1, p. 6]. Reprinted with permission.

Figure 2.1 shows the various stages of filling and emptying of the cylinder, which is illustrated in (A)-(D).

In 2.1 (A) the trapped air and fuel charge above the piston in the combustion

chamber is being ignited by the spark plug, this produces a rapid rise in pressure and temperature which drives the piston down on the power stroke. Below the piston new air and fuel charge is sucked in to the crankcase [1, p. 7].

In 2.1 (B) above the piston the exhaust port has been opened. This point in the cycle is often called the "release point". This allows the hot, highly pressurized combustion byproducts to vent out through the exhaust ducts. [1, p. 7].

In 2.1 (C) the process which is usually referred to as the "blowdown" process is nearing it's end. With the piston uncovering the transfer ports, the cylinder becomes connected to the crankcase through the transfer ducts. If the crankcase pressure exceeds the cylinder pressure then exhaust gases are pushed out of the cylinder and replaced with fresh air-fuel mixture for the next combustion cycle in what is known as the scavenge process.

Whats important to note is that, if the transfer ports are directed badly, the fresh air/ air- fuel mixture will also be directed out through the exhaust, this process is called "short circuiting"[1, p. 8].

In 2.1 (D), in the cylinder, the piston is approaching what is known as the "trapping" point. The scavenge process has been completed at this point and the cylinder is now filled with the new air and fuel mixture. As the piston rises , the cylinder pressure is also rising, but at this point the exhaust port is still open, unless there is an unexpected burst of gas or pressure in the exhaust pipe, there will be some spillage of fresh air/fuel charge into the exhaust port. After the exhaust gas is sealed off, the piston compresses the mixture and it's time for the engine to ignite [1, p. 8].

In shorter terms, a two-stroke engine works on both sides of the piston. Above the piston is where the fuel burns to create power, bellow it, in the crank case, the engine sucks in and prepares the next batch of air and fuel mixture [1, p. 8].

2.2 Noise sources in a simple two-stroke engine

Figure 2.2 illustrates the the noise sources coming from a two-stroke engine. The most noticeable ones are the exhaust and the intake. It's a common misconception that the exhaust port is the noisier of the two, which in it self is true, however the most elementary of exhaust silencers will leave the intake port as the noisier of the two, which means that the inlet must also be silenced to the same degree if not further [1, p. 546].

Furthermore, if the intake system contains a reed valve, a valve which restrict the flow of fluids to a single direction, it produces its own high frequency noise component[1, p. 547].

Vibrating surfaces can acts as a noise source. In the case of the two-stroke engine, the vibrations from bearings, combustion forces and pressure rise are transmitted through the walls and ultimately radiates as airborne noise [1, p. 547].

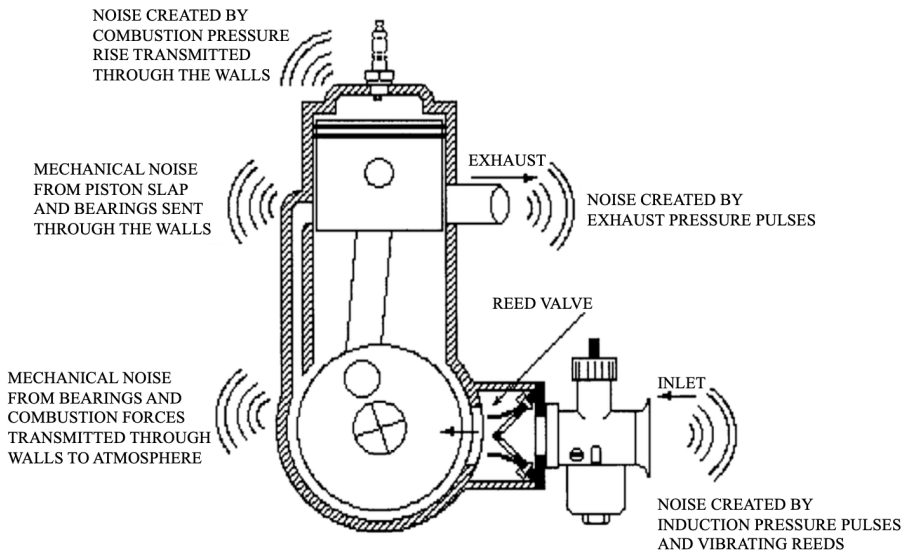


Figure 2.2: Various noise sources radiating from a two-stroke engine [1, p. 546]. Reprinted with permission.

2.3 Side branch Resonators

Side branch resonators are frequently used for reducing low frequency noise. Their configuration and mechanism for sound reduction vary [8]. This part of the theory will introduce different side branch resonators and explain their mechanism.

2.3.1 Helmholtz resonator

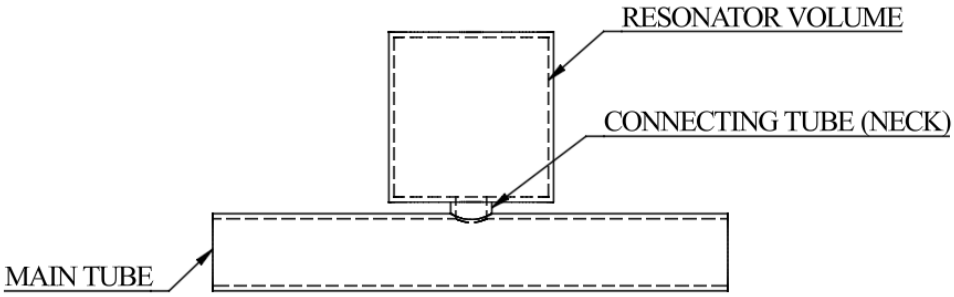


Figure 2.3: Configuration of a Helmholtz resonator

A widely used type of side-branch resonator is the Helmholtz resonator (HHR) [8]. Figure 2.3 shows the configuration of a HHR resonator. The resonance frequency for the HHR is given by the the following expression:

$$f_0 = \frac{c}{2\pi}\sqrt{\frac{S}{V(l_h + \frac{\pi}{2}b)}} \tag{2.1}$$

Where ,b, is the neck radius, l_h, is the length of the neck, S is the surface area of the opening, V is the resonator volume, and ,c, is the speed of sound in the medium.

Whenever a sinusoidal force acts on air in the volume, the air in the neck will be compared to a mass oscillating on a spring. The air in the cavity serves as the spring and handles and provides the system's stiffness element. Due to its contact with the neck's wall, the mass of air in the neck will experience thermo-viscous losses, and this friction makes a part of the acoustic energy be converted into heat [9].

2.3.2 Quarter wave tube resonator

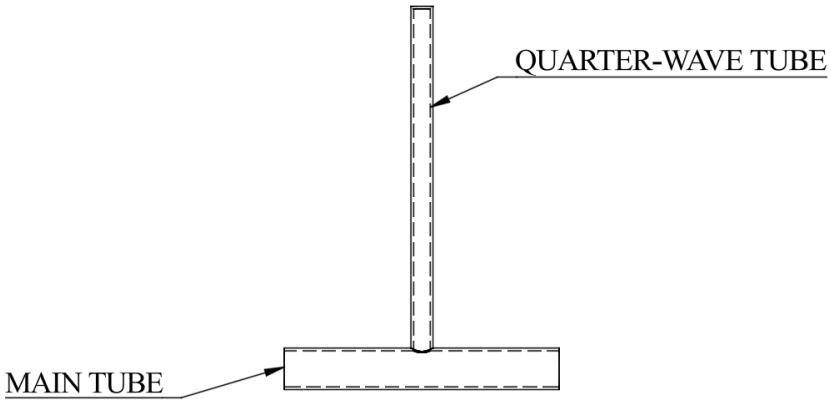


Figure 2.4: Configuration of a QWT

Another widely used type of side-branch resonator is the quarter wave tube (QWT) [8], as seen in Figure 2.4. It is constructed with one open end, which connects to the main duct, and one closed end. At resonance, the wave entering through the open end is reflected at the closed end and meets the incoming wave in the main duct with a phase shift of 180° [10]. This results in cancellation at the resonator's open end, effectively attenuating the sound through destructive interference [8].

The resonance frequency of a QWT is as follows:

$$f_{QWT} = \frac{nc}{4L_{eff}}, \qquad n = 1, 3, 5 \cdots \tag{2.2}$$

where, n, is the harmonic order (odd integers only), c, is the speed of sound and L_{eff} is the effective length of the QWT that includes end effects.

These QWT resonators provide attenuation at odd muliples of the fundamental resonance frequency,($f_1, 3 \times f_1, 5 \times f_1 \cdots$) [11].

The speed of sound is defined as:

$$c = \sqrt{\frac{\gamma RT}{M}} \tag{2.3}$$

Where

- $\gamma = 1.4$ is the ratio of specific heat that is applicable both for diatomic molecules and air.
- R = 8.314 J mol^{-1} K^{-1} is the molar Universal gas constant.
- M = 0.02857 kg mol^{-1} is the average molar mass.
- T is the gas temperature in Kelvin. This is particularly useful as the temperature in the port is higher than room temperature.

For an engine rotating at a constant speed and load, the excitation frequency will stay constant and thus the required length will remain the same [11].

2.3.3 Combining the QWT and the Helmholtz resonator

Wu et al. (2024) introduce a new side branch resonator based on the theory of QWT and HHR, combining the advantages of both mechanisms. The geometry of the hybrid resonator consists of a rectangular resonance cavity connected to the main duct via a short cylindrical neck. The cavity length L is determined by QWT theory, while the cavity volume V is determined independently by Helmholtz resonator theory. This dual dependency provides two separate tuning handles, resulting in a broader effective noise elimination frequency band than either classical design achieves alone.

The cavity length is computed from the modified QWT resonance condition, including the Rayleigh end-correction [12]:

$$L \approx \frac{c_0}{4f_0} + \frac{8r}{3\pi} \tag{2.4}$$

where c_0 is the speed of sound, f_0 is the target resonance frequency, and r is the neck radius. The neck length l_c is constrained to [12]:

$$r \leq l_c \leq 4r \tag{2.5}$$

The lower bound ensures the neck is not so short that wall effects dominate, while the upper bound preserves the lumped-mass assumption that underpins the Helmholtz resonator model. The required cavity volume is then derived from the Helmholtz resonance equation [12]:

$$V = \frac{c_0^2 r^2}{4 l_c f_0^2 \pi} \tag{2.6}$$

and the cavity cross-sectional dimensions, height and width, are obtained from [12]:

$$a \times b = \frac{V}{L} \tag{2.7}$$

A practical constraint on the cavity aspect ratio a/b must be observed. If the ratio becomes too large or too small, the fundamental assumption that cavity dimensions are significantly smaller than the acoustic wavelength is violated. In the limiting case where the ratio becomes too small, transverse waves become dominant inside the cavity and strong three-dimensional acoustic effects emerge at the neck-cavity junction, reducing the accuracy of the lumped-parameter model [12].

2.4 Muffler

There are two principal muffler types, reactive/ reflective and dissipative/ absorptive mufflers, but the possibility to combine the two types exists.

Reactive mufflers attenuate sound through destructive interference. The muffler geometry is designed so that sound waves are reflected back towards the source, where they partially cancel the oncoming pressure waves. Reflection occur at every cross sectional area discontinuity, and a greater number of discontinuity yields a greater attenuation [13].

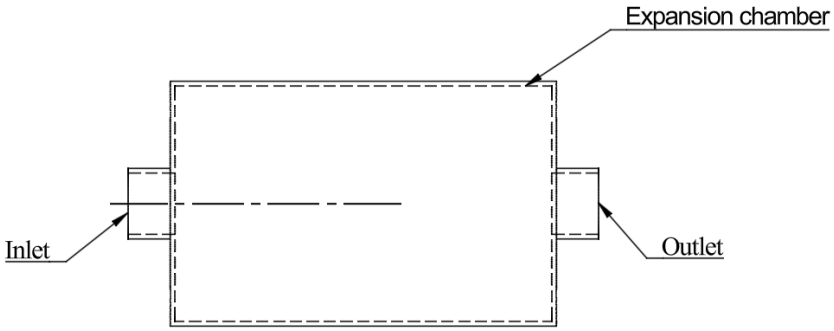


Figure 2.5: Simple expansion chamber

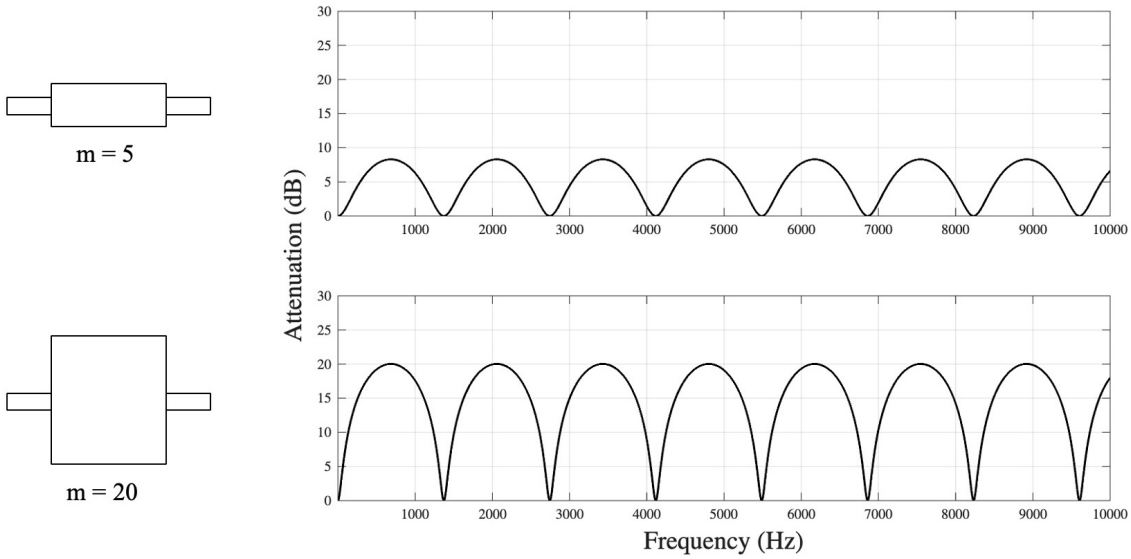
The simplest form of reactive muffler is an expansion chamber, as shown in Figure 2.5. The area discontinuities in this type of muffler interfere with the incident waves, thereby attenuating the transmitted sound. Expansion chambers are most effective at low frequencies [13].

The attenuation in dB of a single expansion chamber is given by:

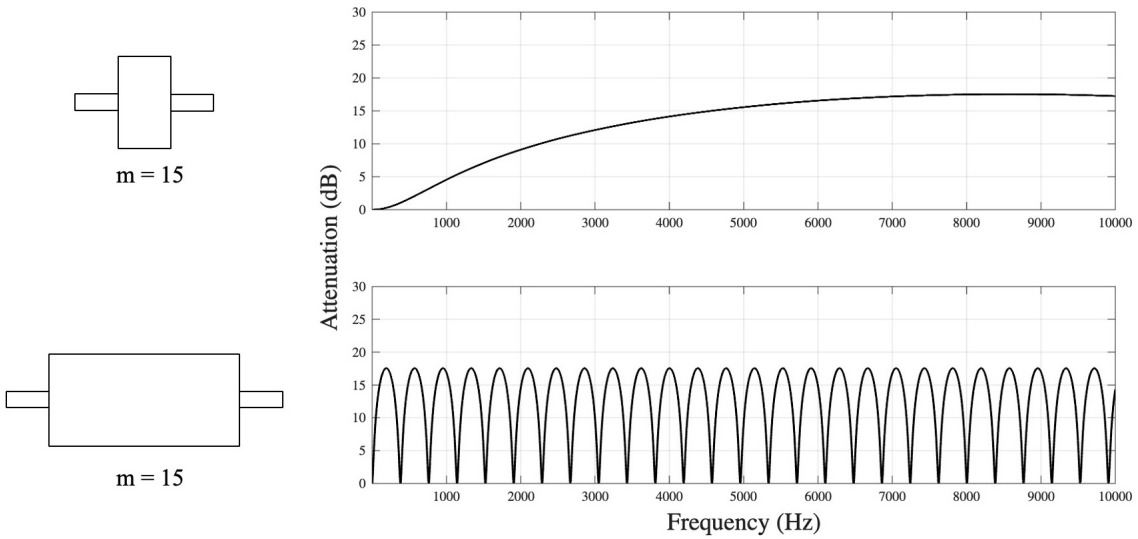
$$\text{Attenuation} = 10 \log_{10} \left[1 + \frac{1}{4} \left(m - \frac{1}{m} \right)^2 \sin^2 k l_e \right] \tag{2.8}$$

Equation 2.8 shows that the attenuation increases with a higher expansion ratio, $m = S_2/S_1$, i.e. the ratio of the chamber cross-sectional area to that of the inlet tube, and that the attenuation curve is cyclic, repeating itself at frequency intervals

determined by the length of the muffler l_c and the velocity of sound inside the muffler, $k = \frac{2\pi f}{c}$ [14, p.85-87], as seen in Figure 2.6.



(a) Effect of expansion ratio m.



(b) Effect of chamber length l_c.

Figure 2.6: Theoretical effect of expansion ratio,m, and chamber length,l_c, on the attenuation.

Absorptive mufflers dissipate acoustic energy as heat by passing sound waves through a porous medium. The typical construction consists of a straight perforated inner pipe which the gases flow through, surrounded by a layer of sound absorptive material such as mineral wool or fiber glass, enclosed within an outer housing as seen in Figure 2.7. The sound radiates outwards through the perforations and is attenuated by viscous and resistive losses in the material inside the housing. The straight through design allows for minimal back pressure, which inherently affects the engine performance less [13].

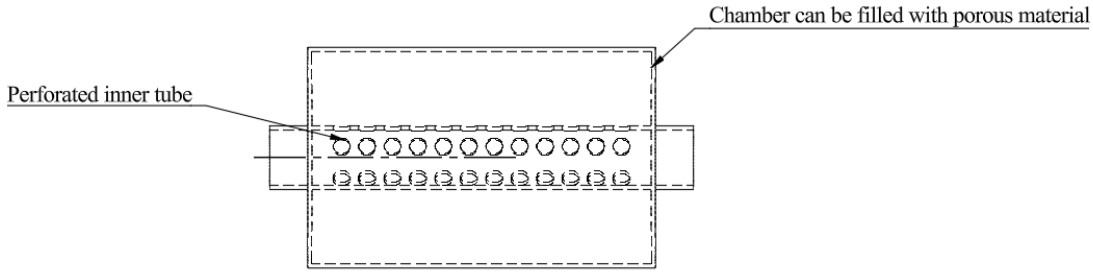


Figure 2.7: Absorptive muffler

Absorptive mufflers provide consistent broadband attenuation, particularly effective at higher frequencies, whereas reactive chamber tend to exhibit narrower attenuation bands. Adding absorptive packing to a reactive chamber improves high frequency performance and smooths the otherwise peaked transmission loss curve [13].

2.5 Plane Wave Propagation

At low frequencies, sound in a circular duct propagates as plane waves, the simplest possible mode of acoustic propagation. In this regime, the acoustic pressure is equally distributed across any cross section of the duct, meaning there is no variation in pressure in the radial or circumferential directions. All acoustic energy travels along the duct axis.

This corresponds to the $m = 0,\ n = 0$ mode, where m is the number of pressure nodal diameters and n is the number of pressure nodal circles across the cross-section. For the plane wave, both are zero, i.e. there are no nodal lines, and the pressure distribution is a constant across the duct face.

2.5.1 Higher Order Modes

The wave equation in a circular duct, expressed in cylindrical coordinates, is [15, p.545]:

$$\frac{d^2p}{dr^2} + \frac{1}{r}\frac{dp}{dr} + \left(k^2 - \frac{m^2}{r^2}\right)p = 0, \tag{2.9}$$

whose general solutions involve Bessel functions of the first kind,

$$p \sim A\, J_m(kr), \qquad k \neq 0, \tag{2.10}$$

where A is a constant, k is the transverse wavenumber and m determines how many nodal diameters exist. Each combination of m and n defines a distinct mode shape with its own transverse pressure pattern. These higher order modes only become able to propagate above a certain threshold, the cutoff frequency [15, p.545].

2.5.2 Cutoff frequency

The cutoff frequency for mode (m, n) in a circular duct of diameter D is

$$f_c = \frac{\alpha_{mn}\, c}{\pi D}, \tag{2.11}$$

where c is the speed of sound and α_{mn} is the value of kR (transverse wavenumber $\times$ duct radius) satisfying the hard-wall boundary condition,

$$J'_m(\alpha_{mn}) = 0. \tag{2.12}$$

The values of α_{mn} for the lowest modes are listed in Table 2.1.

Table 2.1: Values of $\alpha_{mn} = k_{mn}R$ for selected modes in a circular duct.

m	n	α_{mn}	Mode description
0	0	0	Plane wave
1	0	1.84	First asymmetric (azimuthal)
2	0	3.05	Second asymmetric
0	1	3.83	First radial (circularly symmetric)
3	0	4.20	Third asymmetric

The First Asymmetric Mode ($m = 1,\ n = 0$) has one nodal diameter and is the first to become propagating as frequency increases. Its cutoff occurs at $\alpha_{10} = 1.84$, giving

$$f_{c,10} = \frac{1.84\, c}{\pi D} = \frac{0.586\, c}{D}, \qquad \lambda_c = 1.71\, D. \tag{2.13}$$

This is the true plane-wave limit for a circular duct or expansion chamber. Above this frequency, plane wave theory may no longer accurately describe sound propagation.

The First Radial Mode ($m = 0,\ n = 1$) has one nodal circle and a considerably higher cutoff at $\alpha_{01} = 3.83$:

$$f_{c,01} = \frac{3.83\, c}{\pi D} = \frac{1.22\, c}{D}, \qquad \lambda_c = 0.82\, D. \tag{2.14}$$

This mode is only the relevant limit in systems where geometry suppresses asymmetric modes, for example an expansion chamber with a perfectly axially centred inlet and outlet [15, p.547].

2.5.3 Effect of Mean Flow

In the presence of mean flow with Mach number M_a, all cutoff frequencies are reduced by the factor [15, p.548]:

$$f'_c = f_c \left(1 - M_a^2\right)^{1/2}. \tag{2.15}$$

2.6 Transmission Loss in ducts

The transmission loss (TL) is the difference between the sound power of the incident wave entering, and the sound power of the transmitted wave exiting the system, when the system termination is anechoic.

$$TL = 10log_{10}(\frac{W_i}{W_t}) \tag{2.16}$$

Where W_i is the incident power and W_t is the transmitted power [16].

2.7 Insertion loss

Silencer acoustic efficiency is usually assessed by the insertion loss (IL), the unit is dB and it is defined as:

$$IL = L_{W1} - L_{W2} = 10log_{10}(\frac{W_1}{W_2}) \tag{2.17}$$

where, W1, Lw1 and W2, Lw2, is the radiated sound power before and after the implementation of the acoustic silencer [17].

2.8 Technical Framework

To ensure measurement reliability and reproducibility of the noise measurements, this study adheres to ISO 22868:2021. The standard provides a specific noise test code for portable hand- held forestry machinery, utilizing an "Engineering method" (grade 2 accuracy) to determine both sound power levels and emission levels at the operators position.

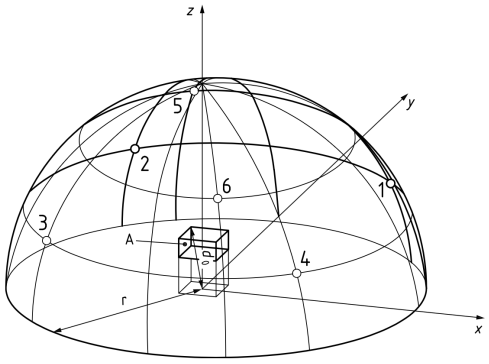


Figure 2.8: Microphone positions on hemisphere, A is the reference box, d0 is the characteristic source dimension, r is the hemisphere radius $\geq$ 2d0 [2, p. 3]. Reprinted with permission.

For sound power determination, the standard specifies a hemispherical measurement surface with six fixed microphone positions, as shown in Figure 2.8. This configuration provides results comparable to larger arrays while maintaining practical measurement efficiency.

For chainsaws, Annex A prescribes a controlled test setup in which the machine is mounted on a rigid stand. The guide bar and saw chain are placed in a standardized test timber without contact, while a loading device (e.g. a water brake) maintains the engine at maximum power speed. Measurements are conducted over defined operating modes, typically idling, full load, and racing—to calculate an equivalent noise level representative of typical use [2].

3

Methods

3.1 Baseline acoustic profile

Figure 3.1 presents the average SPL emitted from the chainsaw across the six microphone positions specified in [2]. The blue line represents the total SPL including the exhaust pipe contribution, while the red line shows the average SPL with the exhaust silenced to such a degree that the intake is assumed to be the dominant noise source.

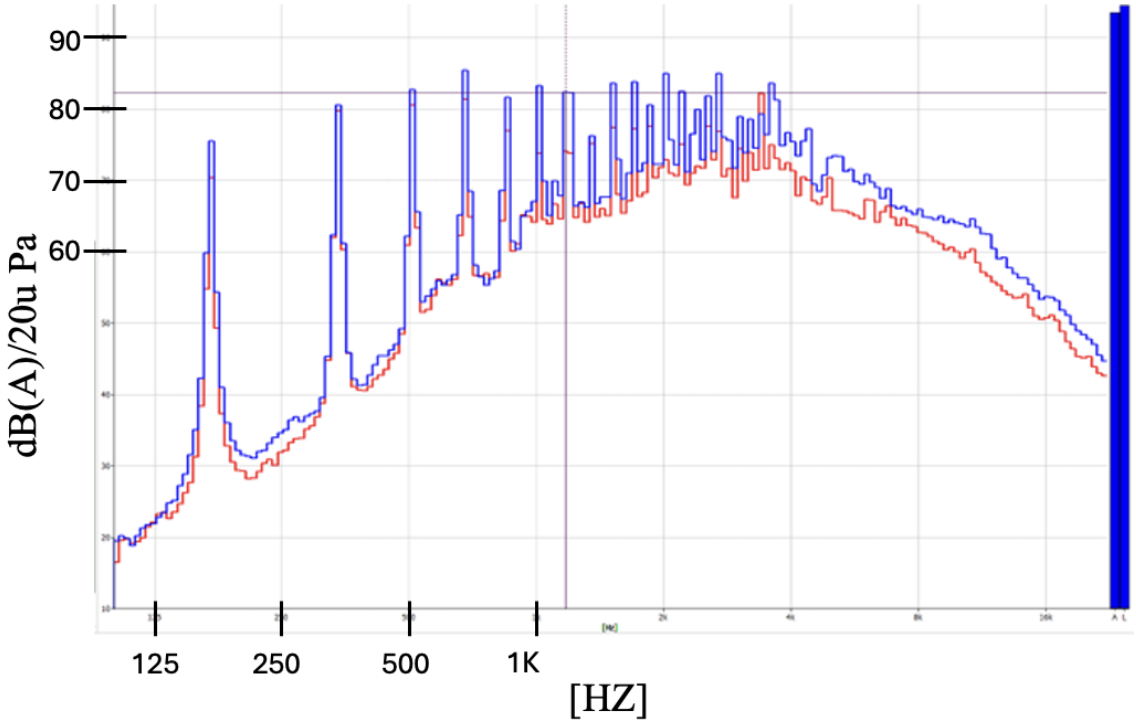


Figure 3.1: Average A-weighted SPL emitted from the chainsaw, measured in accordance with ISO 22868:2021 [2]. The blue line shows the average SPL including the exhaust contribution, the red line shows the average SPL with a heavily silenced exhaust pipe. By courtesy of Fredrik Wibling.

It should be noted that even with the exhaust silenced, isolating the intake contribution is not straightforward. Combustion noise, structure borne noise, and fan noise

all contribute to the radiated SPL. However, in line with the theoretical argument that a sufficiently silenced exhaust leaves the intake as the dominant noise source as stated in [1, p. 546], the red line is taken as representative of intake radiated noise.

The measurements were conducted at full engine load, 170 rps, which also corresponds to the first engine order. Higher engine orders fall at integer multiples of this fundamental, 340, 510, 680 Hz, and so on. Examining the red curve, the second, third, and fourth engine orders are the most prominent peaks, with the fourth order at 680 Hz being the most dominant. At higher frequencies, an increase in SPL is observed around 2.8 kHz. As this does not coincide with any integer multiple of the fundamental engine order, it is likely attributable to a separate source, such as the blade passage frequency or a structural resonance.

Since all three engine orders contribute significantly to the overall sound pressure level, achieving an appreciable broadband reduction requires attenuation across this entire frequency range. The design proposals developed in the following sections therefore target the engine orders falling below 1 kHz, focusing primarily on the fourth engine order at 680 Hz.

3.2 Initial Simulations

As an initial step, the intake port and duct were simplified and modeled as a cylindrical duct with an incident wave excitation at the inlet and a radiation condition at the outlet. This simplified model was used to evaluate the TL and IL produced by different noise reduction measures, such as resonators or mufflers.

The simulations were carried out in COMSOL Multiphysics using the Pressure Acoustics physics interface. All simulations were performed in the frequency domain.

The intake port was excited using COMSOL's port excitation with a constant amplitude of 1 Pa and mode numbers (0,0), corresponding to plane wave propagation, as described in 2.5. Alternatively, the inlet could be excited using COMSOL's plane wave radiation condition, which generates a plane wave with constant pressure while assuming the standard acoustic properties of air in the duct, namely a speed of sound, c, of 343 m/s and an air density, ρ_0, of 1.2 kg/m^3. Both excitation methods produced identical results. Fortunately the frequency range of interest to attenuate for the intake is low enough so that equation 2.13 is generally satisfied.

In the initial simulations, all noise reduction measures were designed to attenuate the 4th engine order, corresponding to 680 Hz, which was shown in section 3.1 to be the most critical frequency in terms of radiated SPL.

The dimensions of the main intake duct are a radius (r) of 6.5 mm and a length (L) of 100 mm.

These dimensions were selected because they correspond closely to one of the ducts in the actual intake system. The full intake geometry will be described in more detail in later simulations.

3.2.1 Quarter wave tube

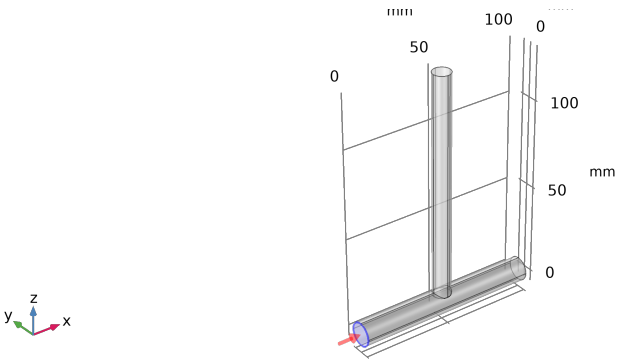


Figure 3.2: QWT coupled to main duct

Figure 3.2 Shows the modeled QWT in COMSOL. This QWT was modeled to attenuate the fourth engine order. It's clear that a QWT requires a large length in relation to the main intake pipe, for practical reasons the resonators are bent in many cases and looped to save the space, which will be needed in the case of the chainsaw as well. Therefore 2 studies were conducted when analyzing the effectiveness of the QWT.

The first study was regarding the bending of a QWT, three different QWT were modeled:

- One straight QWT with 0° bend.
- One QWT with a 90° turn, curved gradually with a 15 mm centerline radius.
- One QWT with a sharp 90° bend.

The three QWT models are shown in Figure 3.3.

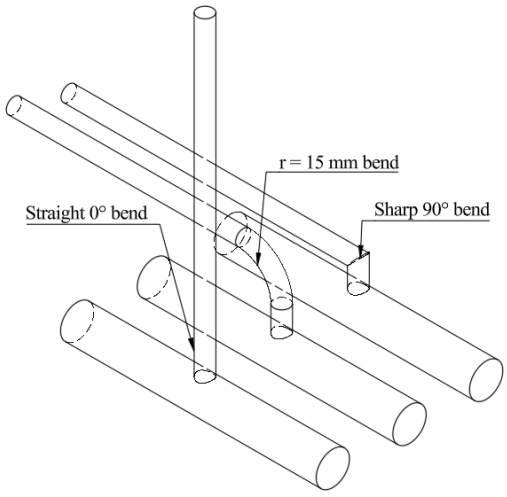


Figure 3.3: Schematic of the three QWT geometries evaluated: straight (left), 90° bend with 15 mm bend radius (centre), and sharp 90° bend (right).

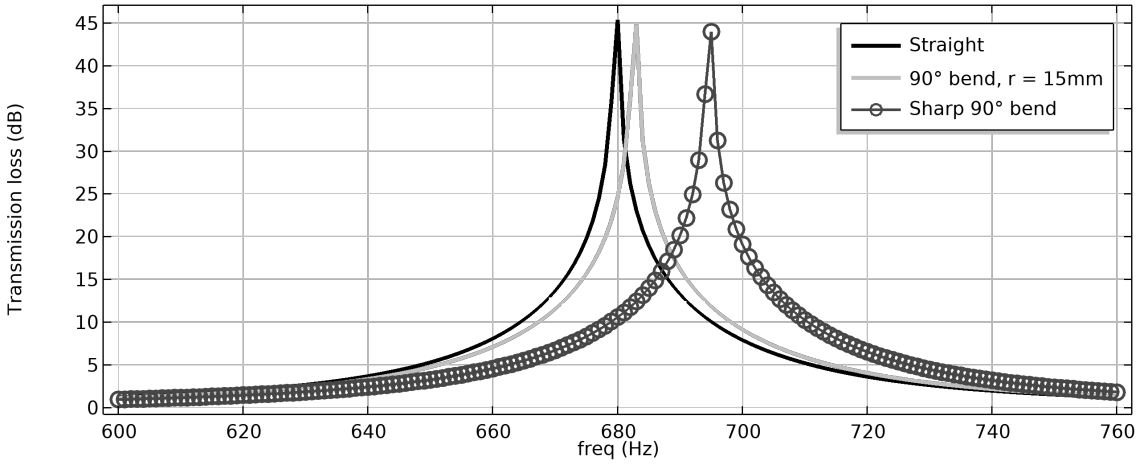


Figure 3.4: Transmission loss for three QWT with different angles of bending, 0, 15, 90 degrees

Figure 3.4 shows the simulated result. As observed bending a QWT inherently does not affect the effectiveness of acoustic attenuation, however it does create a frequency shift, meaning that for this specific case, bending a QWT would require a longer QWT length.

The second phase of the study investigated the geometric relationship between the resonator opening and the cross-sectional area of the main duct. Three specific area ratios were simulated, where the resonator opening area corresponded to 10%, 50%, and 90% of the main duct's cross-sectional area.

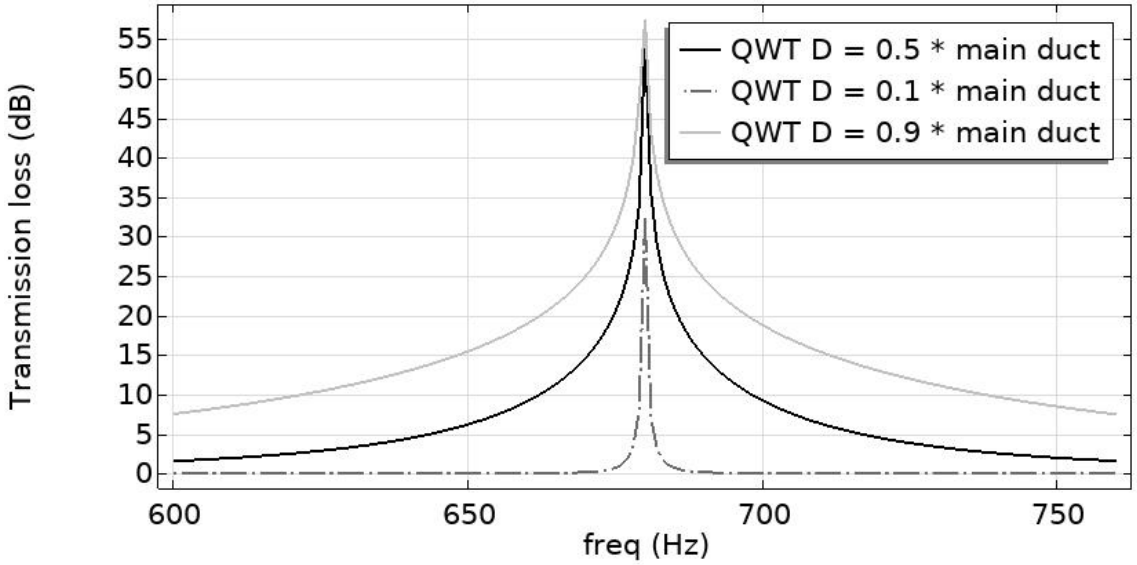


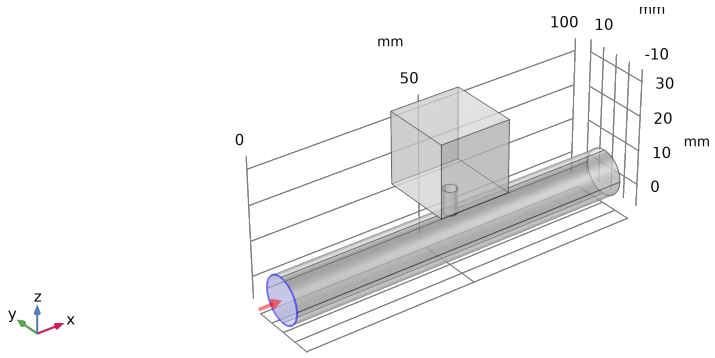
Figure 3.5: Simulated TL for QWT with different resonator opening surface areas in comparison to main duct surface area

Figure 3.5 illustrates the acoustic performance across these three configurations. Unlike the previous study, the physical length of the QWT was adjusted in each simulation to account for end correction. This compensation ensures that all three

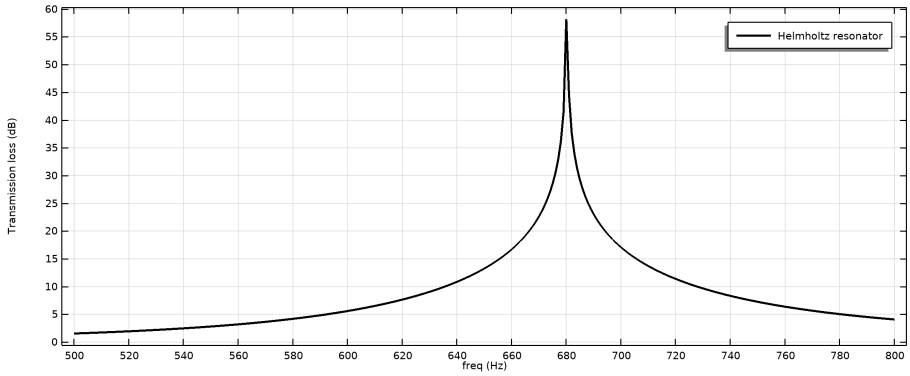
resonators maintain a consistent resonance frequency, isolating the effect of the opening radius on the resulting attenuation.

The results indicate that even a small resonator opening (10%) provides a significant attenuation in TL, however, the attenuation is characterized by an extremely narrow bandwidth. While increasing the opening area significantly enhances effectiveness, there is a point of diminishing returns. Comparing the 50% and 90% area ratios, the peak Transmission Loss remains relatively consistent, whereas the broader opening primarily serves to increase the effective bandwidth of the damping.

3.2.2 Helmholtz resonator



(a) Helmholtz resonator modeled in COMSOL



(b) Corresponding TL cure for Helmholtz resonator

Figure 3.6: TL curve for Helmholtz resonator initial simulations

The second configuration evaluated in the simulations was the HHR, as seen in figure 3.6. The figure shows the modeled HHR in COMSOL with it's corresponding TL curve. This simulation was excited with the same parameters as previous simulations.

As expected the TL curve for the HHR is characterized by a narrow peak at its resonance frequency, which in this case has been tuned to the fourth engine order, 680 Hz.

3.2.3 Combining the quarter wave tube and Helmholtz resonator

The last configuration of a resonator simulated was the combination of the QWT and the HHR as described in 2.3.3. Following the design instruction and exciting the system as it has been for the two previous simulation, the TL provided by the hybrid resonator was computed.

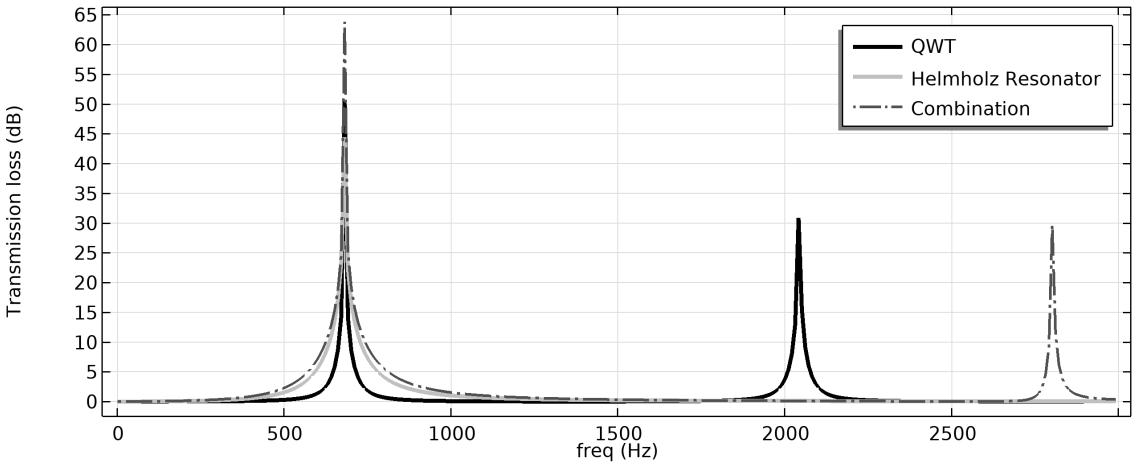


Figure 3.7: Comparison of simulated TL for three different resonator types, QWT, Helmholtz resonator and a combination of the two.

In theory, this hybrid resonator should have a broader attenuation curve than the regular Helmholtz resonator or the QWT. Observing Figure 3.7 it's shown that the hybrid/combination resonator gives a broader attenuation characteristic, while also showing a QWT behavior of having more than a single peak in TL, like the Helmholtz resonator has.

3.2.4 Optimizing the placement

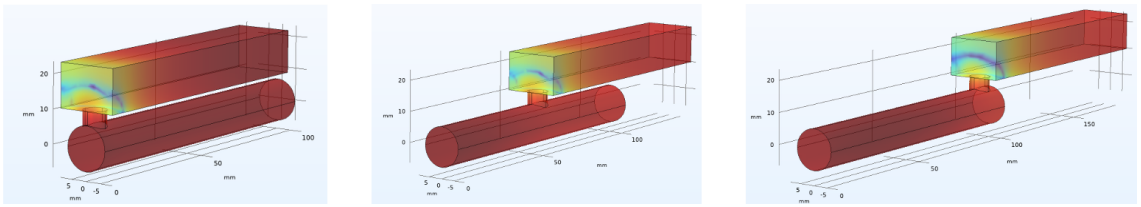


Figure 3.8: Resonator placed on different positions, close to the incident port, in the middle of the duct and lastly at the end of the simplified intake duct where the acoustic wave leaves

The placement of the resonator was also simulated in the early design stage to evaluate the difference in TL caused by placement. In order for the resonator to be effective within the duct, it's necessary to place the resonator at a location in the duct where the pressure is the largest, i.e. a pressure antinode [9].

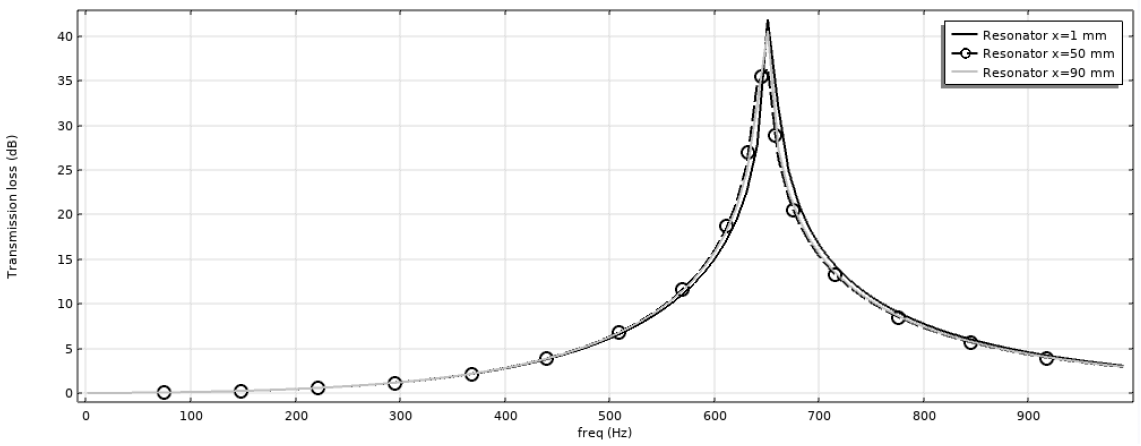


Figure 3.9: Transmission loss of a resonator depending on placement along main duct in x direction.

Figure 3.9 shows the difference in TL depending on the placement of the resonator on the pipe. The resonator was placed in three different positions, 1 mm away from the incident port, in the middle of the duct and 90 mm away from the incident port, i.e at the very end of the duct. As observed in 3.9 there's a stronger TL placing it near the incident port or in the end of the duct. Placing the resonator in the middle of the duct gives the worst TL. There is a difference of 5 dB in TL depending on the placement of the resonator along the duct.

3.2.5 Muffler

The final noise reduction measure simulated in COMSOL involved three muffler configurations, each designed with dimensions comparable to those of the chainsaw intake duct. The three designs were:

1. a simple expansion chamber (Figure 3.10).
2. an expansion chamber with a perforated inner tube and an empty cavity.
3. an expansion chamber with a perforated inner tube and a porous acoustic lining, with a flow resistivity of $\sigma = 5000$ Pa $\cdot$ s/m^2.

The transmission loss (TL) curves for each configuration are presented in Figure 3.11.

For the simple expansion chamber, the intake and outlet ports each have a radius of 6.5 mm and a length of 10 mm. The expansion chamber itself has a radius of 25 mm and a length of 80 mm. This gives an approximate m-value of 14.8. As mentioned in 2.4, m, is the ratio between the surface area of the duct and chamber. The two absorptive muffler configurations (with and without porous material) share the same chamber dimensions, with the inner perforated duct having a radius of 6.5 mm and a total length of 100 mm.

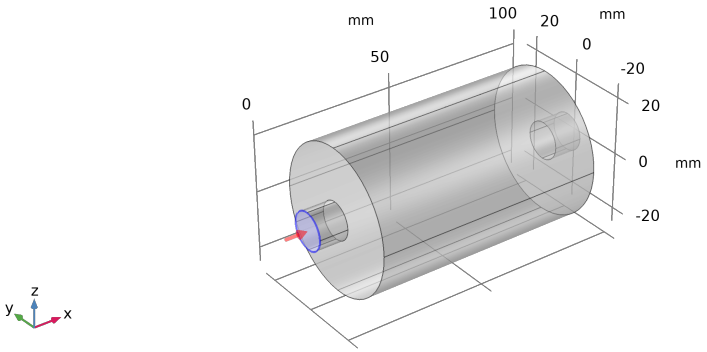


Figure 3.10: Simple expansion chamber modeled in COMSOL.

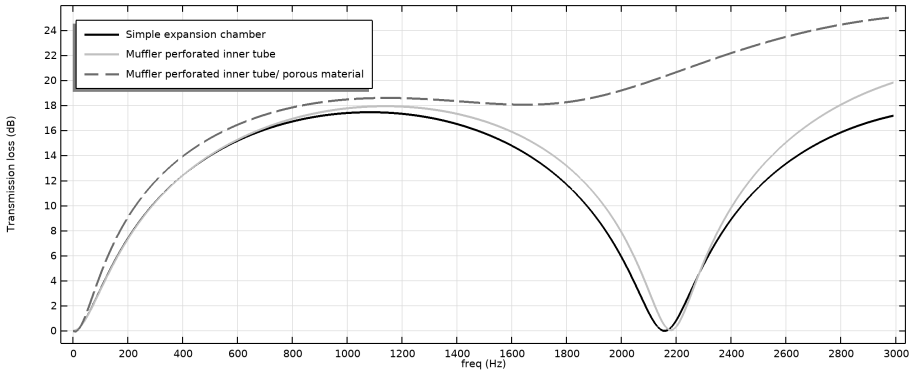


Figure 3.11: Simulated TL for each muffler configuration.

The simple expansion chamber produces a characteristic TL curve as shown in figure 2.6 , exhibiting maxima at frequencies given by:

$$f = \frac{nc}{4L} \tag{3.1}$$

where $n = 1, 3, 5, \ldots$, c is the speed of sound, and L is the chamber length. For the simulated chamber length of $L = 80$ mm, the first maximum occurs at approximately 1071 Hz ($n = 1$), with subsequent maxima at odd multiples of this frequency. Transmission loss minima occur at $n = 0, 2, 4, \ldots$, with the first minimum at approximately 2143 Hz ($n = 2$).

Ideally, the attenuation maximum should coincide with the fourth engine order at 680 Hz, as this is the frequency of interest. This would require a chamber length of approximately 125 mm, a length that exceeds the physical constraints of the intake. Consequently, the resonance frequency could not be tuned to the target value, and a geometric compromise was adopted.

Introducing a perforated inner tube without porous fill yields a similar response, but with increased attenuation at higher frequencies. Adding porous material to the chamber eliminates the attenuation minima and produces progressively greater attenuation with increasing frequency.

3.3 Intermediate simulation stage

The intermediate simulation stage was the second stage in the simulations. For this the geometries were changed, to represent the intake duct more accurately. The dimensions are displayed in 3.12. The most suitable and best performing noise reduction measures, which were shown in the initial simulation stage, were applied to this duct.

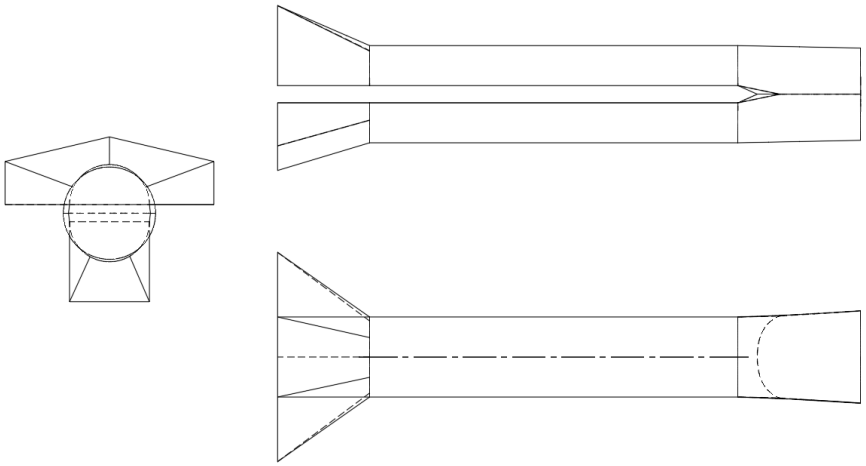


Figure 3.12: Intake port geometry used for intermediate simulations stage

As shown in Figure 3.12, the intake consists of two ducts. The bottom duct, with the smaller port opening, supplies the cylinder with the fuel–air mixture, while the upper duct, with the larger port opening, supplies fresh air only.

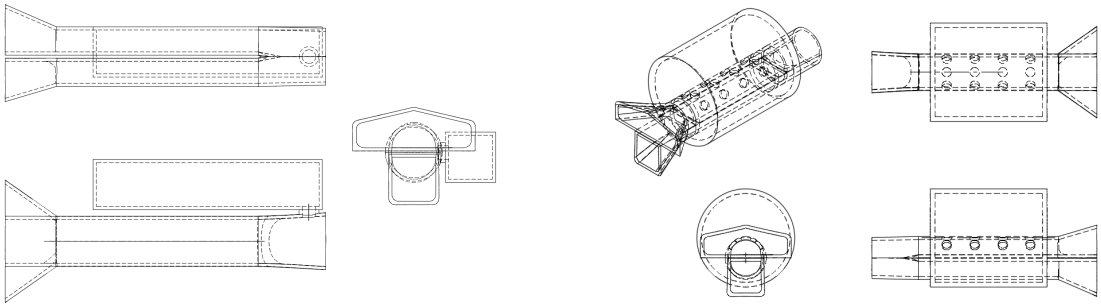
As two sets of measurements were planned ,see Section 3.6, two corresponding sets of simulations were computed, differing only in the point of excitation applied to the system.

In the first set, the port connecting the cylinder and the intake duct was excited by a constant pressure of 1 Pa amplitude. The resulting total SPL was measured at a point 5 cm from the end of the intake duct.

In the second set, the geometry was extended to include the small cone body through which the signal passes before entering the intake duct. This was done to assess the influence of including the upstream signal source on the simulated response. The cone was chosen for this purpose rather than the full engine cylinder and crankcase, primarily due to the relative simplicity of its geometry.

3.3.1 Design proposals

From the simulations in the early design stage two design proposals were further evaluated. The first one being a hybrid resonator utilizing the combination of HHR and QWT geometries as shown in figure 3.13a.



(a) Design proposal of resonator on intake duct

(b) Design proposal of muffler

Figure 3.13: Intermediate design proposals of noise reduction measures on main pipe.

The Resonator is placed at the end of the duct, which was established as a good placing for the resonator to be in section 3.2.4. Furthermore, placing it at the end ensures that it is at a position where the two ducts connect, meaning it can effectively attenuate the contribution from both ducts rather than just one.

The second proposal, being the chamber is shown in figure 3.13b. The diameter of the expansion chamber is 40 mm and the length of the chamber is 50 mm. There are perforations on the top part of the air duct, the diameter of the perforations are 4mm each and in total there are 12 perforated holes, resulting in an area porosity of $\sigma_p = 0.123$. In this design, only the air duct was perforated to prevent damage to the fuel intake, thereby maintaining original fuel flow and preserving engine power.

3.3.2 Simulated IL

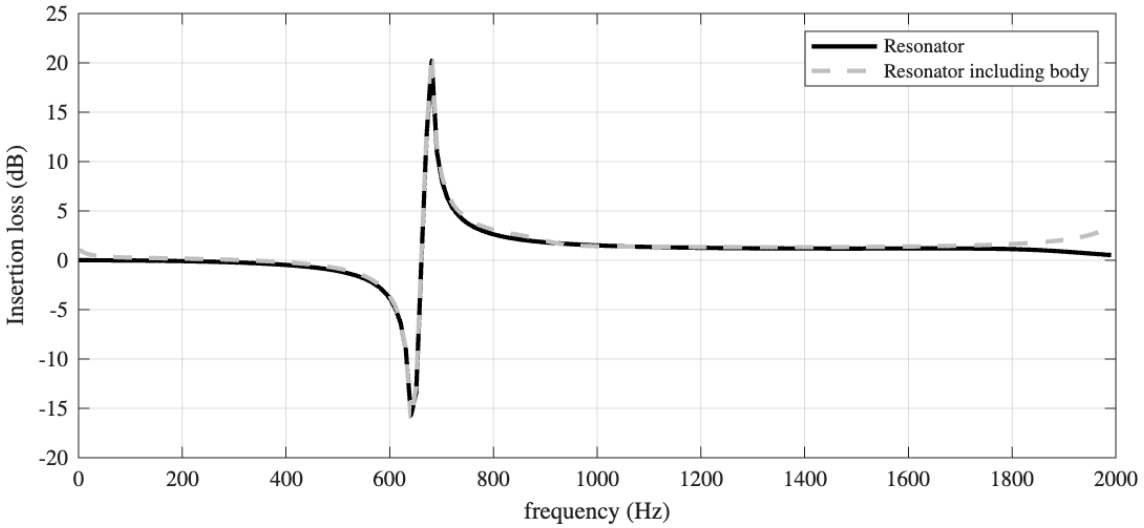
The insertion loss (IL) for each configuration was calculated to quantify the acoustic attenuation achieved by the different design proposals. Since the radiation from the outlet was omnidirectional, the insertion loss was defined as:

$$IL = SPL_{maintube} - SPL_{configuration(n)} \tag{3.2}$$

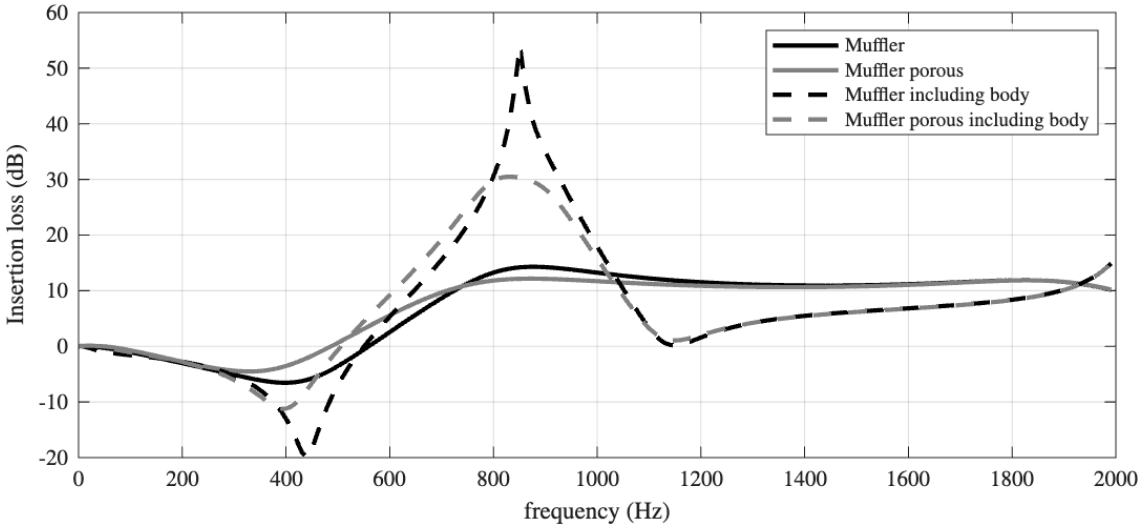
where n=1–3 represents the four investigated configurations:

- Expansion chamber with perforated air head duct.
- Expansion chamber with perforated air head duct and porous material inside the cavity of the chamber.
- Resonator coupled with the main tube.

The simulated insertion loss for each design proposal including and excluding the body of the cone as described in section 3.3, and motivated by 3.6, is shown in figure 3.14.A positive IL indicates sound reduction the configuration is installed, a negative IL indicates amplification.



(a) Simulated IL for the resonator configuration including and excluding the body of the cone



(b) Simulated IL for the muffler configurations including and excluding the body of the cone

Figure 3.14: Simulated IL for the design proposals suggested in the intermediate simulation stage including and excluding the body of the cone which the upstream signal comes from.

It can be observed that the addition of any of the proposed configurations initially introduces a negative effect on the IL. For all configurations, a distinct dip in insertion loss appears before the frequency range where sound attenuation is achieved. This dip represents a local amplification and therefore contributes negatively to the overall sound power level. However, if this amplification does not coincide with dominant engine orders, its impact on the perceived noise and overall performance will be limited.

The resonator configuration exhibits a much narrower frequency response, charac-

terized by one pronounced dip and one peak in insertion loss, this applies for both the simulation model excluding and including the body of the cone. The dip occurs at approximately 640 Hz, which does not coincide with any dominant engine order. The peak in IL appears at approximately 680 Hz and aligns well with the fourth engine order, making it particularly relevant for targeted attenuation.

In contrast, for the muffler configurations, both the attenuation and amplification regions are significantly more broadband compared to the resonator configurations. This indicates that the muffler affects a wider frequency range, both positively and negatively. When porous material is introduced inside the resonator volume, the peaks and dips in insertion loss become less pronounced and smoother, indicating increased damping in the system. A similar damping effect is observed for the muffler when porous material is added.

For the muffler, excluding the body of the cone, the negative IL region (amplification) occurs approximately between 10–480 Hz when porous material is included inside the cavity, and between 10–540 Hz when the muffler is empty. This frequency range overlaps with the first three engine orders, which is unfavorable. However, above approximately 500 Hz, a broadband attenuation is achieved, with an average insertion loss of around 10 dB extending up to 2000 Hz.

For the muffler, including the body of the cone, the amplification region occurs between 10-500 Hz when porous material is included in the cavity, and between 10-550 Hz when the cavity is empty. This, once again, overlaps with the first three engine order which is not favorable. Above the region of amplification the mufflers starts to attenuate. Unlike the simulation model ,with the body of the cone excluded, where the IL became stable around 10 dB, the new simulation model including the cone shows a sharper peak reaching IL values up to 52 dB, although still very broadband. This trend applies to both the muffler with and without porous material in the cavity.

It's shown that including the body which the signal is sent through doesn't effect the simulated IL for the resonator, however it has an impact on the muffler configurations.

3.4 Detailed simulation stage

The third and last stage of the simulations is the detailed stage simulations. In this stage the actual dimensions of the current existing intake were accounted for, furthermore each design proposal made during this stage accounted for the dimensions of the actual chainsaw and that they should fit under the hood. The dimensions of the intake duct for the detailed stage simulation is shown in 3.15.

From earlier stage simulations and measurements it was shown that there are ways to acoustically attenuate the noise level emitted from the intake, both broadband and narrow band, however, due to the time limit only one design proposal was further developed to fit on the actual chainsaw, and that is the resonator. This was also the design proposal chosen due to the fact that the least modification was needed

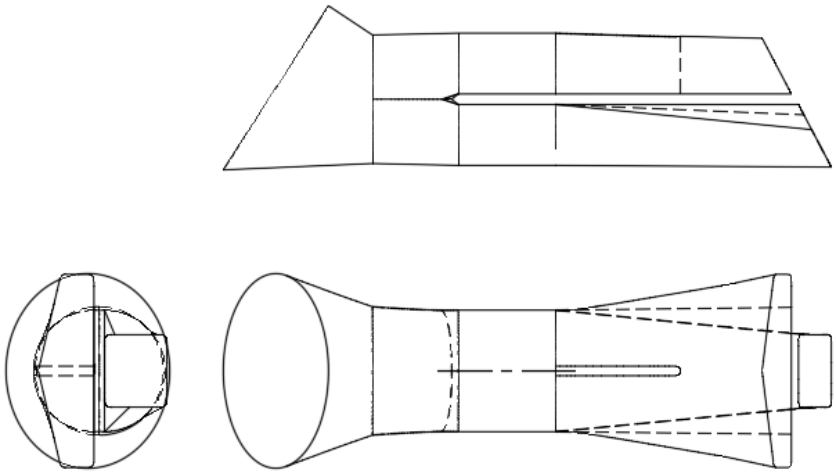


Figure 3.15: Intake port geometry used for detailed simulation stage

on the existing intake duct. Furthermore it was shown, that for this particular case, connecting a resonator to the intake duct did not require including the body which the sound is emitted from, further simplifying the design and also the already heavy computational time required for the simulations.

3.4.1 Detailed design proposal

The resonators were designed using the principle of QWT, where the resonance frequency is determined by equation 2.2. Since these design proposals were to be placed on the actual chainsaw, a higher temperature ($30°C$), i.e. a higher speed of sound was accounted for (351 m/s).

In total 4 design proposals were presented, one resonator designed to attenuate at 680 Hz (4th enigne order), one designed to attenuate 850 Hz (5th engine order), one to attenuate both the 4th and 5th engine order i.e. 680 and 850 Hz. Lastly one to attenuate the 850 and 1020 Hz (5th and 6th engine order).

The resonator was placed at the outlet of the of the intake pipe, where the air filter is to be installed on top of. This was done for a number of reasons. The first being the space available under the chassis of the chainsaw was the greatest at this point of the intake duct. The second being that the placement of the resonator should be at a pressure antinode as stated in [9] and shown in 3.2.4, which it is if placed furthest back at the duct. Lastly this part of the intake duct is made of plastic in real life, making it easy to create different modifications in traditional 3D printing material such as PLA, PETG or SLS without being too concerned regarding material properties.

To ensure the resonators could be accommodated beneath the chainsaw hood, they were bent. This geometric modification is known to induce a shift in the resonance frequency, as shown in 3.2.1. This was accounted for in the design by adjusting the

effective resonator length accordingly.

The resonator opening had a diameter of 6 mm, which can be considered relatively small in comparison to the main duct diameter, which is 28 mm at the point of connection. This potentially limits its acoustic effectiveness. From an acoustic perspective, a larger opening would generally be preferable. However, due to spatial constraints within the system, increasing the diameter was not feasible, and it was therefore maintained at this size.

3.4.2 System excitation

The intake duct in this simulation stage was subjected to two excitation methods. First, a uniform pressure boundary condition with an amplitude of 1 Pa was applied, maintaining consistency with previous stages. While the excitation remained constant, this stage introduced updated geometry and a modified speed of sound to account for elevated operating temperatures.

Second, the intake was excited via a normal velocity boundary condition, simulating a diaphragm-like oscillation with a constant amplitude of 1 m/s. This second configuration utilized the same geometric and thermal parameters as the pressure-driven case to ensure a direct comparison between the two methods.

3.4.3 Detailed stage Simulated IL

The resulting Insertion Loss (IL) from the detailed design stage simulations is illustrated in Figure 3.16.

Figure 3.16 comprises four sub-plots representing the different design proposals:

- **First plot:** IL for the Quarter-Wave Tube (QWT) tuned to 680 Hz (4th engine order).
- **Second plot:** IL for the QWT tuned to 850 Hz (5th engine order).
- **Third plot:** IL for the dual-QWT configuration tuned to 680 Hz and 850 Hz (4th and 5th engine orders).
- **Fourth plot:** IL for the dual-QWT configuration tuned to 850 Hz and 1020 Hz (5th and 6th engine orders).

As anticipated, the IL curves exhibit prominent peaks at the resonance frequencies, validating the attenuation capabilities of each design. Furthermore, it is observed that the choice of excitation, whether constant pressure or constant velocity, does not yield significant variations in the simulated IL, indicating that the predicted performance is independent of the source characterization used in this stage.

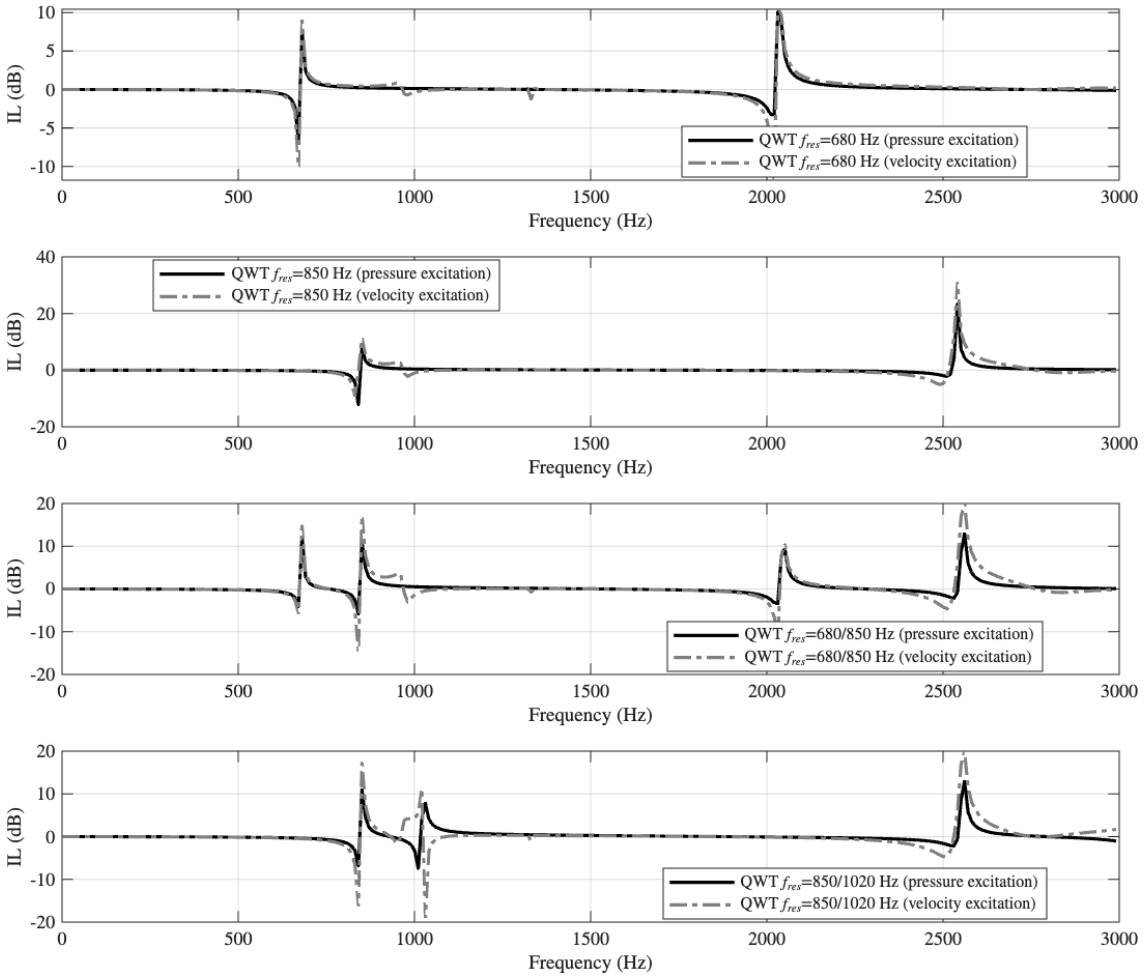


Figure 3.16: Simulated IL from the detailed design stage. The plot compares the IL resulting from pressure-based versus velocity-based excitation at the incident port for each design proposal (QWTs and their corresponding resonance frequencies).

3.5 Tuning/ Troubleshooting the detailed model

As evidenced by both the simulated and measured results presented in Section 4.2, the resonators exhibit insufficient attenuation performance, most notably a failure to attenuate sound at the fundamental frequencies for which they were tuned. A systematic troubleshooting process was therefore conducted to identify potential improvements to the design. Four parameters were investigated. First, the placement of the resonator along the intake duct was evaluated by testing three positions: at the inlet adjacent to the cylinder, at the midpoint of the duct, and at the far end corresponding to the position used in the detailed design proposal.

Second, the influence of resonator geometry was assessed by comparing the performance of the existing bent resonator configuration against an otherwise identical straight resonator, in order to isolate any effect the bend may have on attenuation effectiveness.

Third, the number of QWT resonators coupled to the main duct was varied, with

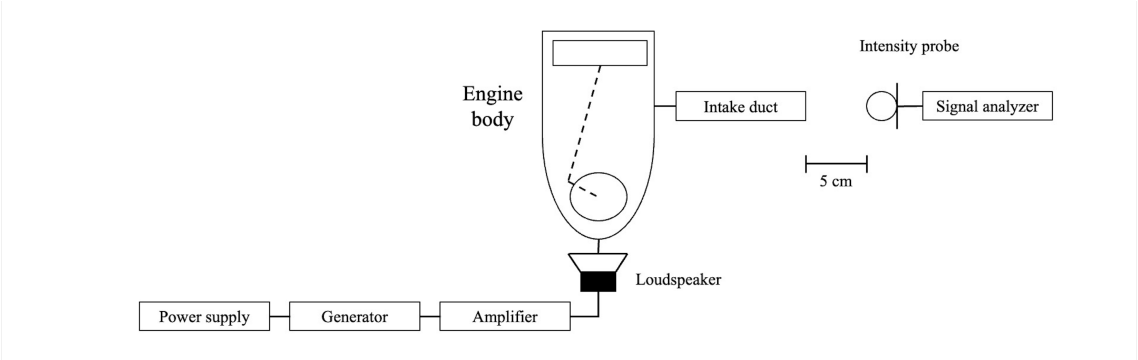
configurations of one, four, and eight resonators examined to determine whether increasing the number of resonators yields meaningful improvements in acoustic performance.

Lastly the geometry of the outlet was investigated. On the true intake, the outlet is coned. This effect was compared to having the outlet straight and cylindrical, to isolate any affects it may have on the system.

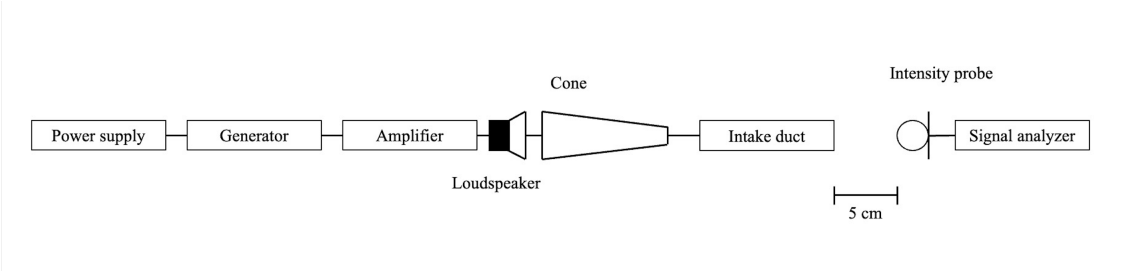
3.6 Validating the design proposals

To validate the attenuation predicted in the simulations, experimental measurements of the system were conducted.

Two measurements were done, the first set of measurement consisted of a loudspeaker being placed below the two-stroke engine radiating sound into the crank house and then being measured at the outlet of the designed intake duct, as shown in Figure 3.17a



(a) Signal sent through the engine body into the intake duct and measured at the outlet



(b) Signal sent through via the cone to the intake and measured at the outlet

Figure 3.17: Measurement setup schematics

The second set of measurements were similar to the first, but rather than the sound wave traveling through the engine into the intake duct, the signal was sent more directly into the system by connecting the loudspeaker via a cone to the intake duct directly, and measuring at the outlet as previously, as shown in Figure 3.17b and 3.18.

For both set of measurement, the same parameters were used. The signal used was white noise, to excite a broad frequency range, with a level of 80 dB in SPL. The output signal was measured 5 cm away from the opening of the intake duct with an intensity probe capturing the pressure, velocity and intensity.

To have as minimal background noise/ leakage from the loudspeaker during the measurements the body which the loudspeaker was sitting in was taped and covered with clay, also absorption material was placed on top of it. The purpose of this, as mentioned was to have as little background noise as possible, but also to have a good signal to noise ratio (SNR) so the measurements could be reliable.

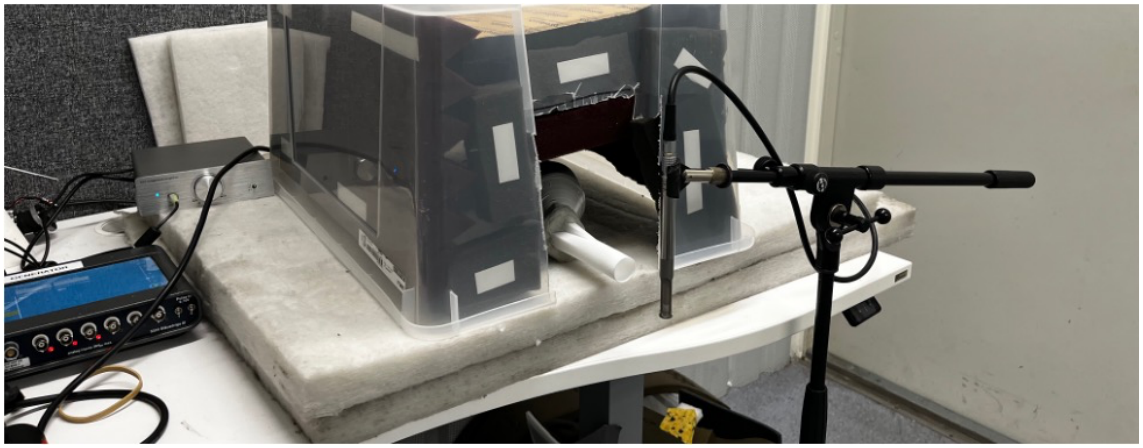


Figure 3.18: Measurement setup

3.7 Design process

Figure 3.19 shows the complete design and validation process used for designing an intake noise reduction component. The flowchart outlines the iterative workflow, from initial simulations through validation and testing on the operating chainsaw. Important to note is that due to the limited time and resources the last step, testing design proposal on chainsaw during running operations, were not conducted. However this is still included in the chart.

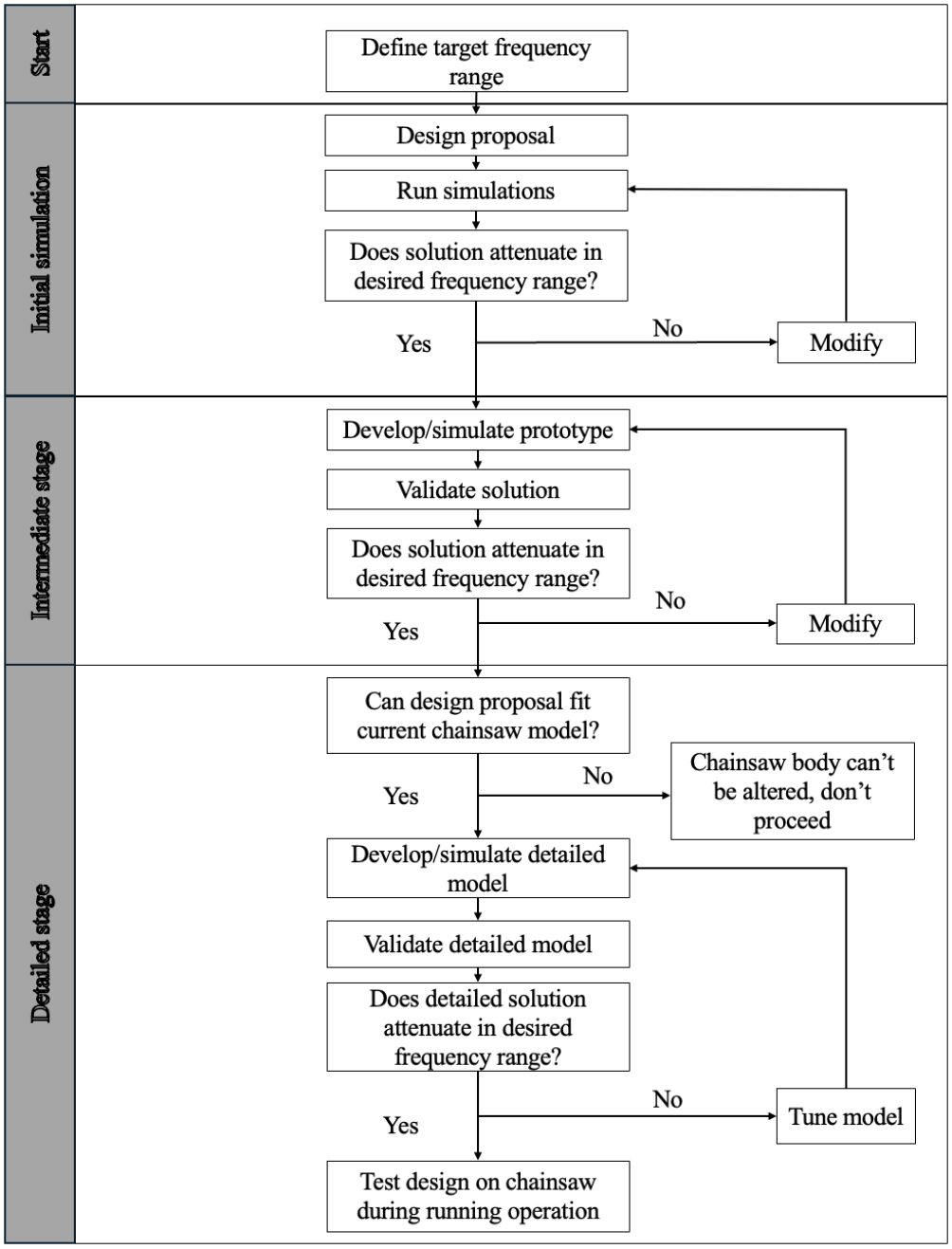


Figure 3.19: Flowchart illustrating the design and validation process for an intake noise reduction component.

4

Results

This Chapter will highlight the results of the findings from validating the design proposals as described in 3.6. Since two sets of measurements were made for the design proposals, the results will be split in to two parts for each design proposal and design stage, the two parts are listed bellow:

1. **Crank house measurements**, where the signal was sent through the crank house and it's response was measured 5 cm away.
2. **Inlet duct measurements**, where the signal was sent through the cone, exciting the inlet duct more directly. The response was measured 5 cm away from the outlet.

The results will be shown in chronological order, beginning with the intermediate design proposals, followed by the detailed design proposals and finally the tuning of the detailed design proposal. Their respective simulations will be included to evaluate the measured results with the theoretical predicted.

The parameter evaluated is the IL to show the acoustic improvement caused by changing the baseline duct.

4.1 Intermediate stage design proposals

4.1.1 Crank house measurements

4.1.1.1 Insertion loss resonator

Figure 4.1 shows the result of the measured IL using the resonator on the main duct compared to the simulated IL for the same conditions,the simulated model did not include the engine body. For the measurements the general trend seems to align well with the simulated IL. The peak in IL still remains at 680 Hz which is what the resonator was designed to attenuate. The simulated IL shows a higher attenuation than the measured, reaching up to 20 dB IL while the measured reaches up to 8 dB. At higher frequencies, the measured system shows fluctuations, specifically two distinct peaks around 1.4 kHz and 1.6 kHz, and a dip around 1.8 kHz. These fluctuations are not predicted by the simulated models.

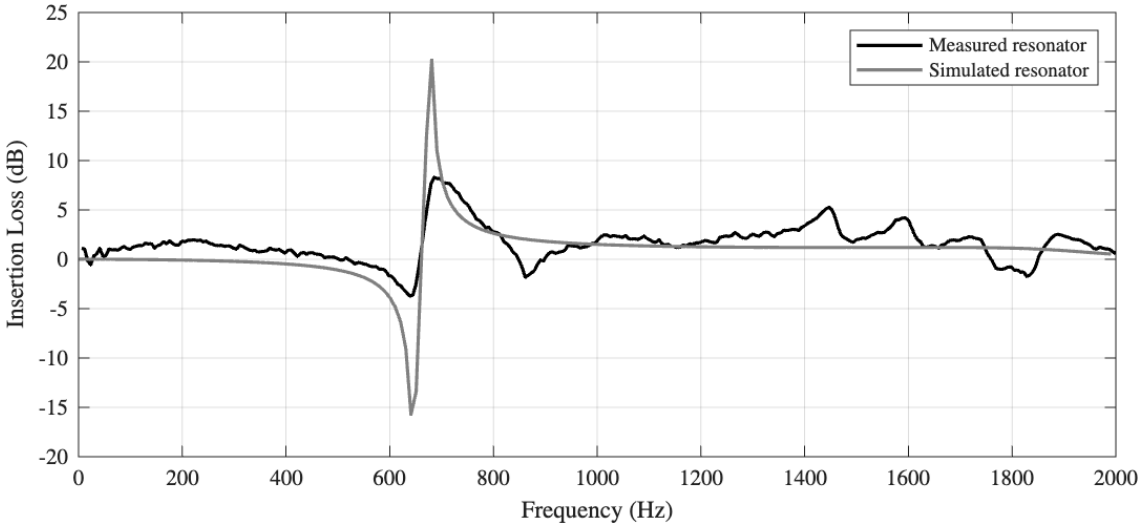


Figure 4.1: Measured and simulated IL for resonator coupled to main duct

4.1.1.2 Insertion loss muffler

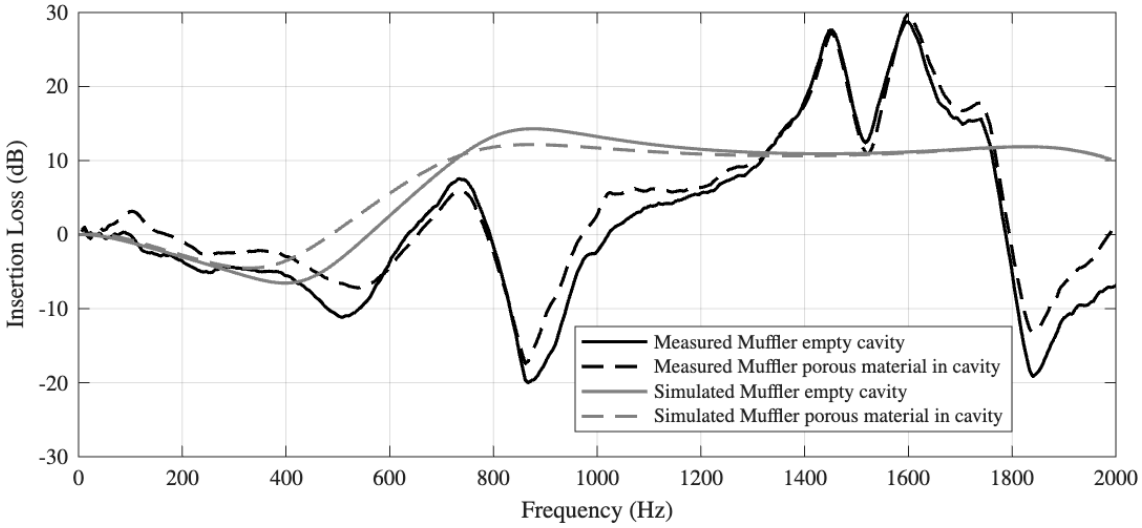


Figure 4.2: Measured and simulated Insertion Loss (IL) for the perforated duct muffler with an empty cavity versus a cavity filled with porous material.

Figure 4.2 illustrates the measured and simulated Insertion Loss (IL) for a muffler featuring a perforated air head duct, comparing an empty cavity configuration against one filled with porous material, once again the simulated model did not include the engine body. In the low-frequency range below 400 Hz, the measured data aligns closely with the simulation, where both show a trend of noise amplification rather than attenuation. As the frequency increases from 400 Hz to 700 Hz, the muffler begins to function as predicted by the simulation, transitioning and attenuating the noise. However, beyond 700 Hz, the experimental measurements and the simulated results begin to diverge significantly. While the simulation predicts a relatively stable and consistent reduction of approximately 10 dB up to 2 kHz, the physical measurements exhibit much higher irregularities.

Specifically, the measured IL for both configurations shows a sharp dip near 900 Hz before climbing to provide strong attenuation, with peaks reaching nearly 30 dB around 1.4 kHz and 1.6 kHz. peaks at these two specific frequencies were also observed in figure 4.1.

The inclusion of porous material appears to dampen the magnitude of these fluctuations, particularly by reducing the depth of the IL dips observed at frequencies bellow 600 Hz and around 1.8 kHz. Despite the lack of alignment between the simplified simulated model and the measured data in the high frequency spectrum, the experimental results confirm that the design proposal achieves effective broadband attenuation in the frequency range 1000- 1800 Hz.

4.1.2 Intake duct measurements

4.1.2.1 Insertion loss resonator

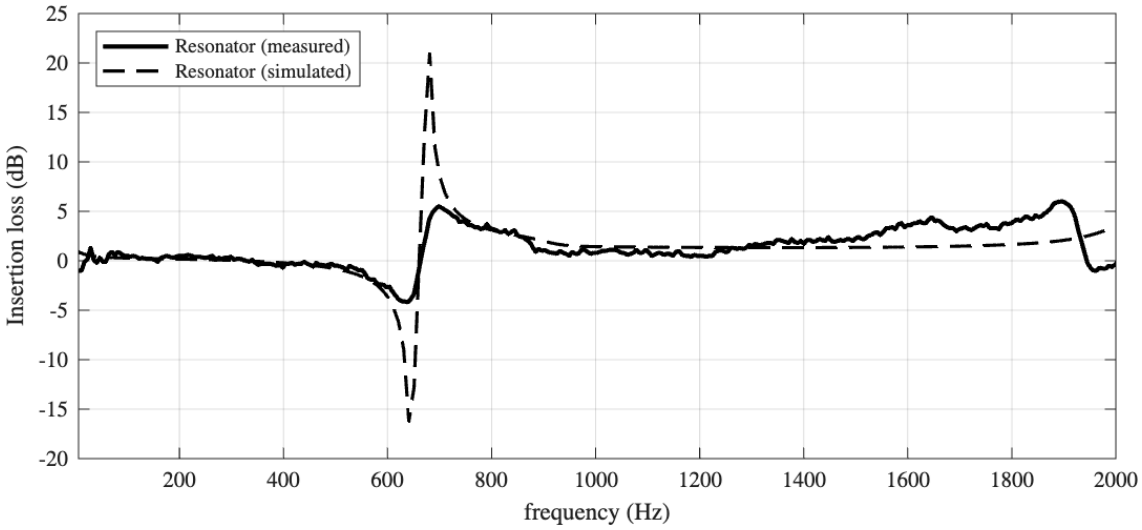


Figure 4.3: Measured and simulated IL for the resonator coupled to the main duct

Figure 4.3 shows the measured and simulated insertion loss (IL) for the intermediate stage resonator proposal, where the signal was sent through the cone . The simulated model included the body of the cone which the signal was sent through. As with the previous measurement and simulation, the resonator attenuates sound pressure over a narrow frequency bandwidth centered at its tuning frequency.

The physical system exhibits less attenuation than the simulation predicts, yet the measured IL still captures a clear attenuation trend, achieving up to 5.5 dB reduction at the targeted fundamental frequency. The simulated IL for the resonator achieves around 20 dB IL.

At higher frequencies, a second IL peak appears in the measured data near 1.9 kHz, the simulated results indicate in the same trend by rising. However there is a frequency shift in where this second peak appears between the simulated and the measured. The fluctuations in frequencies above 1 kHz, specifically 1.4 and 1.6-kHz, which were observed in figure 4.1 are no longer apparent in the measured IL.

4.1.2.2 Insertion loss Muffler

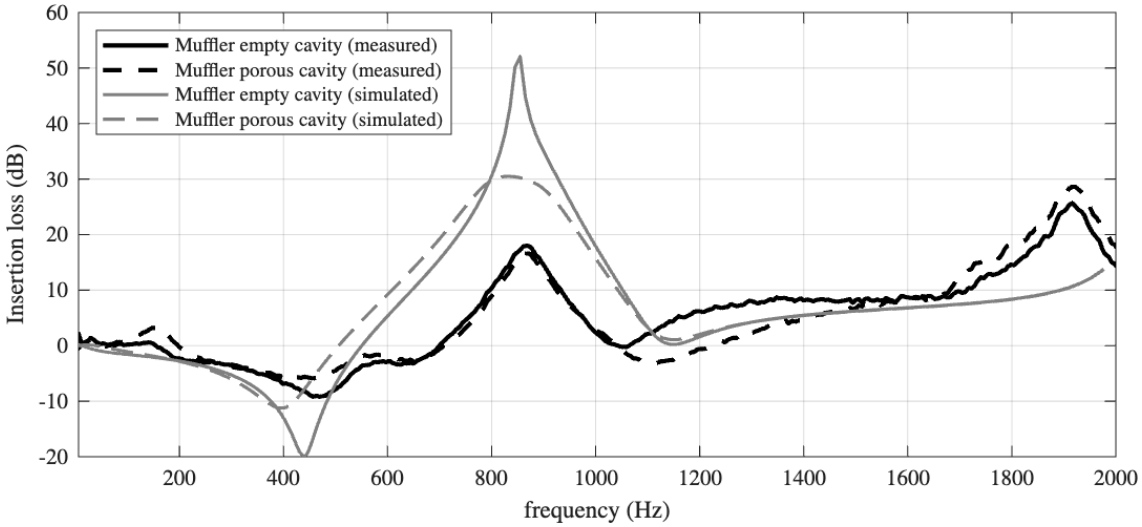


Figure 4.4: Measured and simulated IL for the muffler configurations

Figure 4.4 shows the measured and simulated IL for the two muffler configurations, The body of the cone was included in the simulations.

The general trend between the simulations and the measurements align much better, especially in comparison to the trend alignment in figure 4.2. At low frequencies, sub 500 Hz, the measured IL follows the simulated results and dips down before it starts to attenuate, 600 Hz and upwards. The simulated muffler configuration shows a positive IL value between 500 and 1150 Hz. The measured IL shows a positive IL value between 700 and 1000 Hz. Although not as broadband as the simulations predicted, it's still relatively broad in comparison to the resonator.

In regards to the amplitude of the attenuation provided, the measured system reaches up to almost 20 dB in IL around 850 Hz, both for the muffler with an empty cavity and with the cavity filled with porous material. This is something the simulated model did not predict, in the simulated results the muffler with porous material in the cavity has much lower IL (20 dB lower) in comparison with the muffler with an empty cavity. Furthermore the simulated model predicts a greater IL than what is shown in the measured IL.

At higher frequencies, around 1.9 kHz, a second peak occurs, this peak reaches levels between 25- 30 dB in IL. The simulated result show the same trend of a rise in IL, but in higher frequencies, so there is a shift in resonance between them.

4.2 Detailed model loudspeaker measurements

4.2.1 Crank house measurements

Figure 4.5 presents the measured insertion loss (IL) for the detailed model design proposals together with the corresponding simulated results. It should be noted

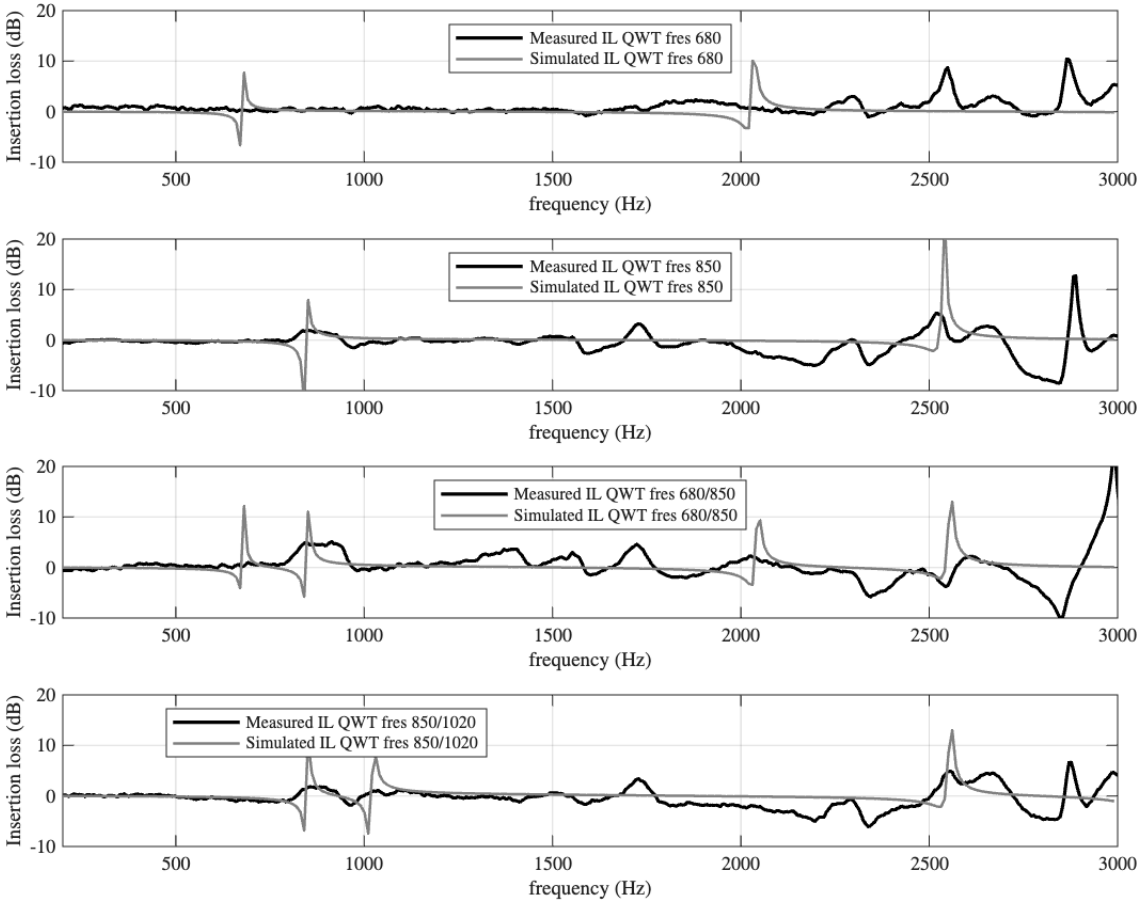


Figure 4.5: Measured and simulated IL for each detailed design proposal. Measurement conducted using Loudspeaker sending signal through crank house through to the intake duct. Signal measured 5 Cm away from intake duct.

that the simulations assume an air temperature of 30 °C in the intake duct, whereas the measurements were conducted at approximately 22 °C. This discrepancy affects the speed of sound and may introduce slight shifts in the resonance frequencies observed between simulation and experiment. In addition, the simulation model does not include the engine body (crankcase, cylinder, piston etc), through which the acoustic signal propagates in the experimental setup, resulting in a simplified representation of the acoustic system.

The first plot shows the IL for the QWT tuned to 680 Hz (corresponding to the 4th engine order). The measured response is noticeably more damped than the simulated result, which is consistent with previous observations. In contrast to the simulation, no clear attenuation peak is observed at the fundamental tuning frequency of 680 Hz. However, at higher harmonics, particularly around 2040 Hz, a slight attenuation can be identified in the measurements, although it is significantly weaker and broader than predicted. Additionally, two distinct dips appear in the measured IL in the frequency range of approximately 2.5–3 kHz, which are not present in the simulation.

The second plot shows the IL for the QWT tuned to 850 Hz (5th engine order).

At the primary resonance frequency, a modest peak in the measured IL is observed, which aligns reasonably well with the simulated result. A second peak appears around 2.5 kHz, however, it is difficult to determine whether this feature is directly related to the QWT or if it originates from the broader system response, as similar behavior is also observed in the previous configuration.

The third plot shows the IL for the combined QWT configuration tuned to 680 Hz and 850 Hz (4th and 5th engine orders). In the simulations, two distinct attenuation peaks are clearly visible at the respective tuning frequencies. In the measured results, these features are less pronounced and appear more broadened. While some attenuation can be observed in the frequency regions around the targeted resonances, the peaks are not as clearly separated as in the simulations. At higher frequencies, above 1 KHz , additional fluctuations in the measured IL are observed, which are not captured by the simulation.

The fourth plot shows the IL for the QWT configuration tuned to 850 Hz and 1020 Hz (5th and 6th engine orders). Similar to the previous case, the simulations predict two distinct and relatively sharp attenuation peaks at the tuning frequencies. In the measured results, these peaks are again present but appear significantly reduced in magnitude and broader in shape. The attenuation effect at 850 Hz is still identifiable, whereas the response around 1020 Hz is less distinct, indicating that the effectiveness of the QWT is reduced in the experimental setup. As in the other configurations, the measured IL exhibits additional features at higher frequencies, particularly around 2.5 kHz and above, which are not reproduced in the simulations. These discrepancies can be attributed to the simplified nature of the model, which neglects damping and excludes the influence of the engine body and other upstream components.

4.2.2 Inlet duct measurements

Figure 4.6 shows the measured and simulated IL for the detailed model design proposal. Once again it should be noted that the accounted temperature was 30 °C, so any frequency shifts in resonance frequency of the simulated IL of the resonators can be accounted to that. The signal was sent through a cone to the intake duct, avoiding the reflections occurring in the body of the engine.

First plot shows the resulting IL for the QWT tuned to 680 Hz. The simulated IL shows two peaks, at the fundamental tuning frequency (680 Hz) and the second peak at the first odd multiple of the fundamental tuning frequency (2040 Hz). The measured IL shows clear visible peak at the first odd multiple of the fundamental frequency, although shifted down in frequency, reaching up to 3 dB IL. This measured IL however is not as strong as the simulated one, which reaches up to 10 dB IL. At the fundamental tuning frequency the measured IL still shows some resonance behavior, amplifying the sound before attenuating, however this effect is very weak.

The second plot shows the measured IL for the QWT tuned to 850 Hz with its corresponding simulated result. The simulated results show two peaks in IL, the first at 850 Hz and the second at 2550 Hz, fundamental tuning frequency and the

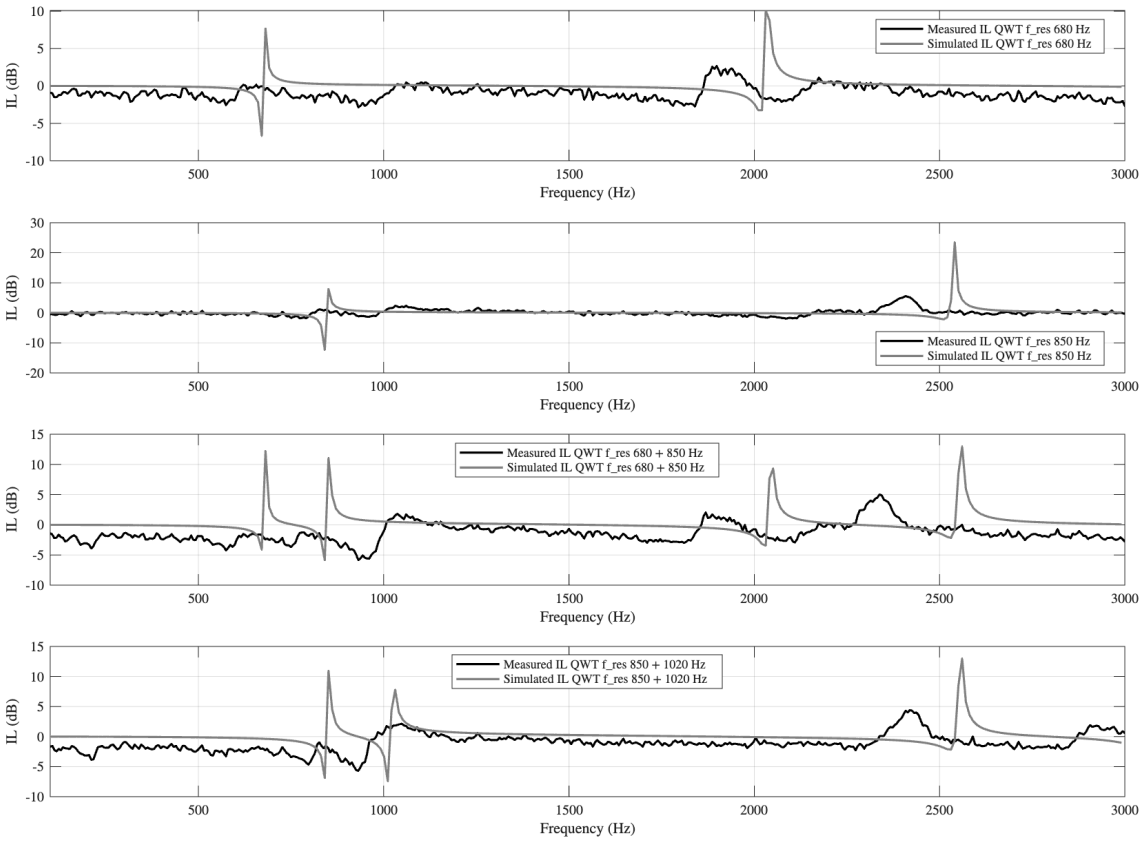


Figure 4.6: Measured and simulated IL. Measurement conducted using Loudspeaker sending signal through cone to the intake duct. Signal measured 5cm away from intake duct.

first odd multiple of the fundamental frequency. The measured IL show a stronger IL peak at the first odd multiple of the fundamental frequency reaching up to 5 dB. At the fundamental tuning frequency for the meaured Il shows a resonating trend but it's far weaker, only reaching up to 0.8 dB.

The third plot shows the measured IL for the detailed model which has two resonator coupled to the systems with two different tuning frequencies, 680 and 850 Hz. The simulated IL shows in this case four peaks in IL, at 680 and 850 Hz along with their corresponding first odd multiple of the fundamental frequency, at 2040 and 2550. The measured IL shows the two peaks at each first odd multiple of each QWT resonator, and a resonating trend at the fundamental tuning frequencies but they are very damped.

The fourth and last plot shows the measured IL for the detailed model which has two resonator coupled to the systems with two different tuning frequencies, 850 and 1020 Hz and their corresponding simulated result. The simulated IL shows three peaks, at the fundamental tuning frequencies 850 and 1020 Hz, and one peak at the first odd multiple of 850 Hz at 2550 Hz. The measured IL shows a clear peak at the first odd multiple of the fundamental tuning frequency of the QWT tuned to 850 Hz reaching up to 5 dB in IL. At the fundamental frequencies the resonating trend

remains both at 850 and 1020 but far more damped.

In general the detailed design proposal show attenuation at the odd multiples of the fundamental tuning frequencies, but at the fundamental tuning frequency they are compromised.

4.3 Experimental tuning design solution

4.3.1 Resonator placement

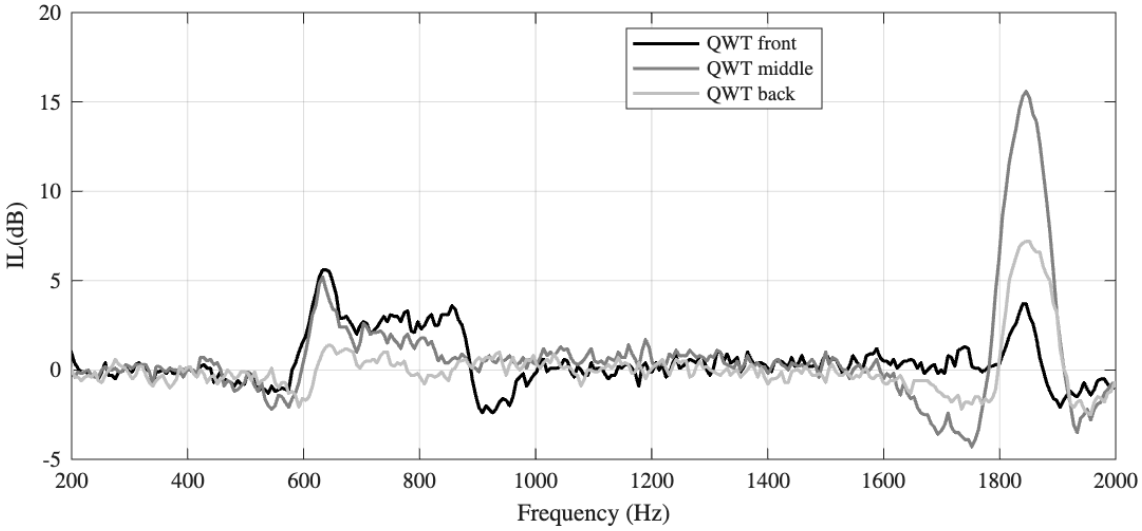


Figure 4.7: Measured Resonator placement

Figure 4.7 Shows the IL for a QWT placed along 3 different positions on the intake duct. The 3 placements are in the "front", which is closest to the cylinder, in the middle of the duct and in the back close to the outlet of the intake duct, this is where the resonator of the detailed design proposal was placed as well.

As shown in the figure it's more beneficial to place the resonator closer to the cylinder rather than placing it further in the back. Placing it in the front or in the middle yields a higher recorded IL (around 5-6 dB) for the first targeted fundamental frequency of 680 Hz. Placing the resonator in the back closest to the outlet of the intake duct yields a IL of only 1.4 dB.

The second IL peak recorded in figure 4.7 however is the greatest for the resonator placed in the middle (up to 16 dB in IL). For the resonator Placed furthest away from the cylinder in the back, this second peak gives an IL of around 8 dB, and for the resonator placed in the front closest to cylinder in the front is around 4 dB.

It should also be noted that placing the Resonator in the front shows a broader dampening in recorded IL, as it gives a positive value of IL from 600 to around 900 Hz.

4.3.2 Number of resonators

Since only one resonator in the back is shown to be insufficient in reducing the IL, the question is how many resonators are needed in the back to produce a substantial IL.

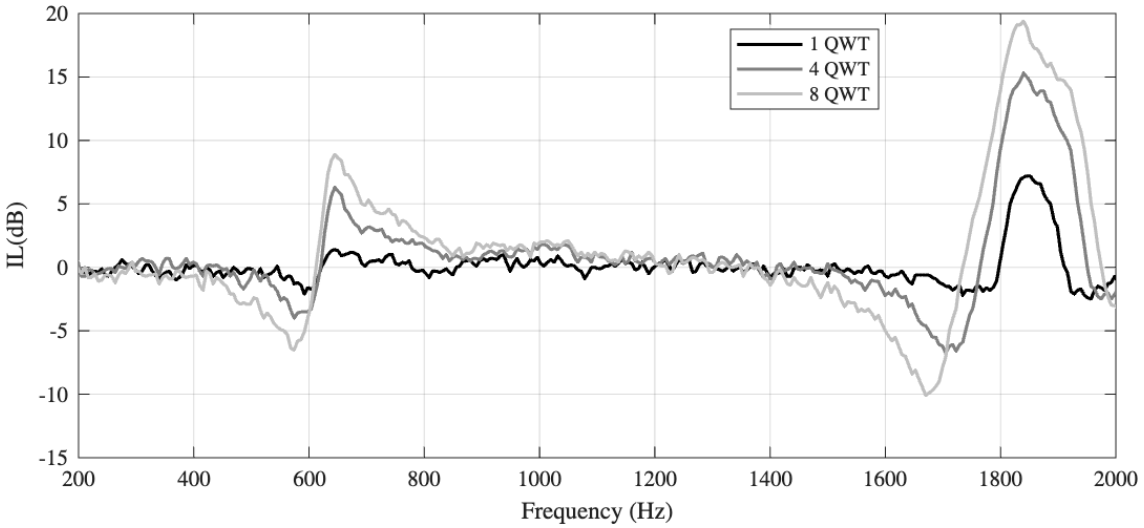


Figure 4.8: Comparing IL of intake pipe with different amount of QWT coupled to the system

Figure 4.8 shows the measured IL using one, four and eight QWT resonators coupled to the intake system. All resonators were tuned to the same resonance frequency and positioned at the same axial location along the duct, but distributed circumferentially around it. As seen increasing the number of resonators in the back provides a greater damping in the system, i.e increasing the number of resonators yields a higher IL value. Increasing the number of resonator not only provides a higher IL value, but also a broader damping effect. This implies to both the first fundamental tuning frequency but also the second peak.

Figure 4.9 compares the effectiveness of one QWT in the front to four QWT placed in the back. Its shown that to get the same effectiveness in the first fundamental resonance frequency of the QWT in the front, four QWT are needed in the back to achieve the same result. However when it comes to the second peak in IL the four QWT give a much higher value of IL.

4.3.3 Bending the resonator

Since the resonators on the detailed model had to be bent to fit under the hood of the chainsaw, the influence of the bending was also investigated experimentally.

Figure 4.10 shows the resulting IL for a straight QWT coupled to the system and a bent QWT. The resonator opening and length were the same for both configurations to only see the effect of bend. As highlighted by the results, bending the QWT did not affect the effectiveness of the resonator at its fundamental tuned frequency.

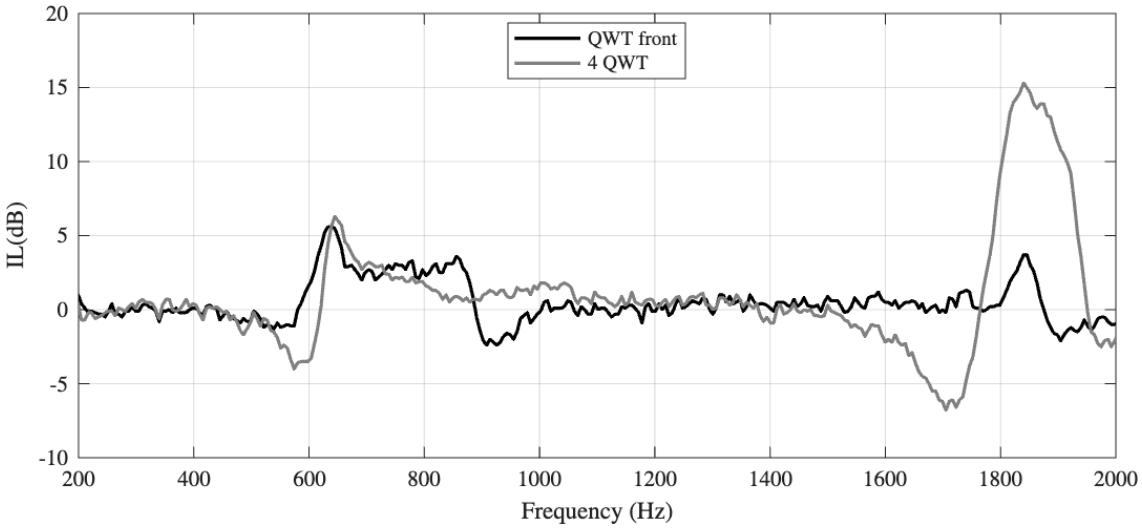


Figure 4.9: Comparison of one QWT in the front and 4 QWT in the back

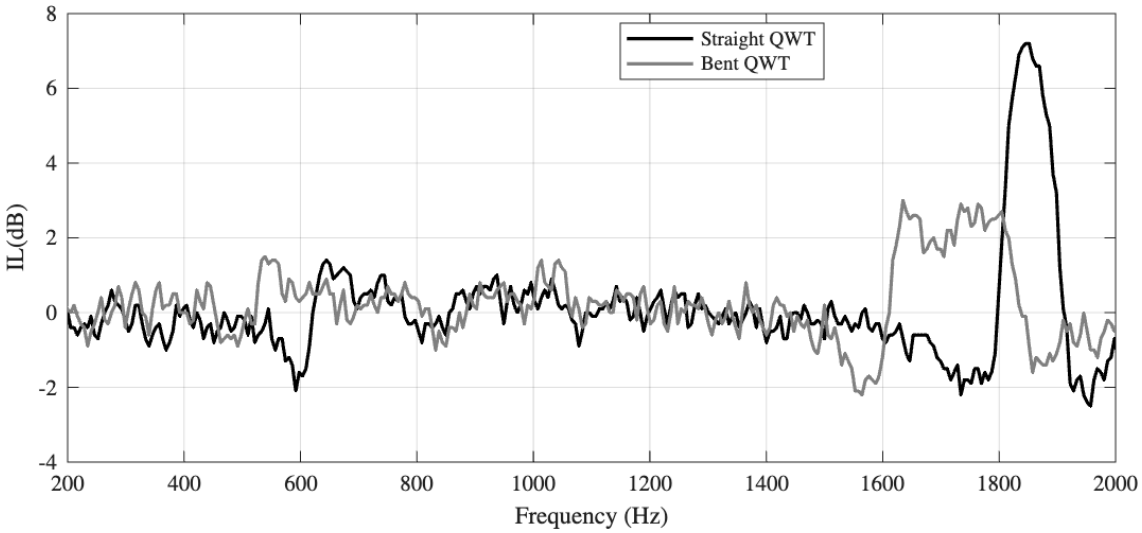


Figure 4.10: Bent QWT compared to straight QWT

However, the resonance frequency of the QWT shifted downward. This result aligns well with the simulated results in 3.2.1, where it was shown that bending a QWT resonator only shifted its resonance frequency.

Looking at higher frequency range, the second peak for the straight QWT and the bent one exhibits behaviors which differentiates more than just a frequency shift. The straight QWT achieves a higher amplitude in IL, up to 7 dB, while the bent QWT reaches an IL of up to 3 dB. There's also a difference how broad the damping is. For the straight QWT it's more narrow than the bent QWT, While the straight resonator attenuates from 1.8 - 1.9 KHz, the bent attenuates from 1.6- 1.85 kHz. This is a difference of 250 Hz.

4.3.4 Piped and coned outlet

The current intake outlet is coned, meaning the the surface area of the intake duct increases as it approaches the outlet, as seen in figure 3.15. The effect of this was also experimentally measured by comparing a QWT placed near the outlet of the intake duct with a coned outlet, and one with a piped outlet, i.e a straight cylindrical outlet that did not increase in surface area.

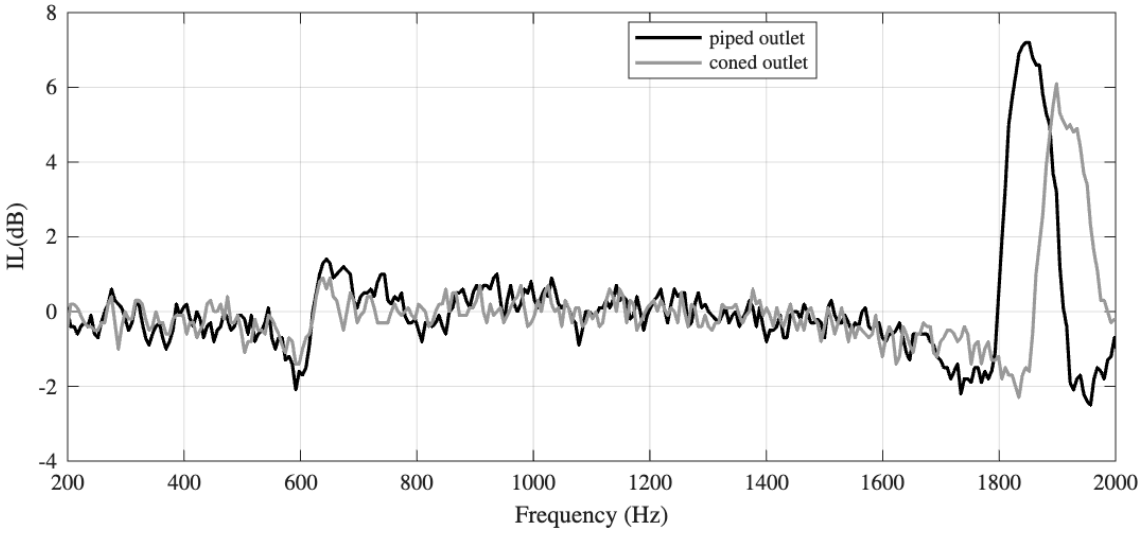


Figure 4.11: Comparison of Piped outlet and straight outlet

Figure 4.11 shows the results of this comparison. Both systems had the same length, opening and positioning of the QWT on the duct. The resulting IL shows a slight difference between having the resonator in the back of a coned outlet intake duct and a piped one.

The difference of he fundamental resonance frequency, around 680 Hz, is very small for the two systems. The piped system achieves a greater measured IL, around 1.5 dB, while the coned system achieves around 1 dB. The second peak in IL shows the same trend of the piped system achieving a higher IL in comparison to the coned system. The piped system reaches an IL value of 7 dB while the coned system reaches an IL value of 6 dB. The coned system, although its well aligned with the piped system in the first peak, at the second peak its shifted upwards in the frequency range.

4.4 Tuning of the simulation model

The simulated model was after the experimental tuned to include damping to improve the results from the simulations, so that they are in better agreement with what the measured result shows.

Figure 4.12 shows the results from the measured IL for one QWT mounted in the front and the corresponding simulated IL for the same configuration, but with damping included. The simulated model is now more aligned with what the measurements

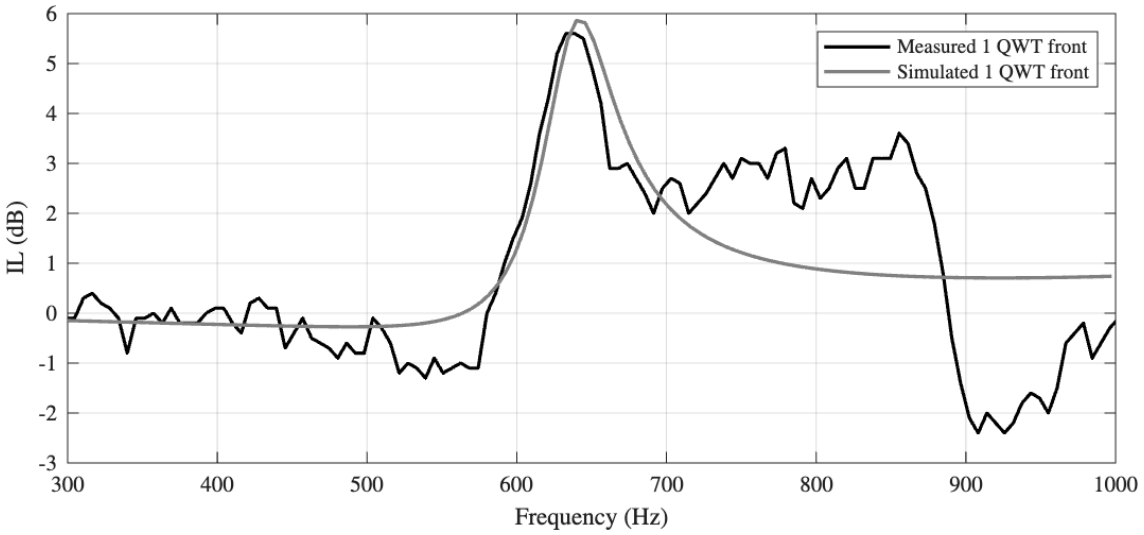


Figure 4.12: Measured IL for front mounted QWT and simulated IL, including damping in simulation model

shows.

Both the measured systems and simulated show a strong peak at the resonance frequency, reaching up to 5.5 dB in IL. The simulated is more ideal IL curve for the QWT, but the overall the magnitude of the IL is fitted well.

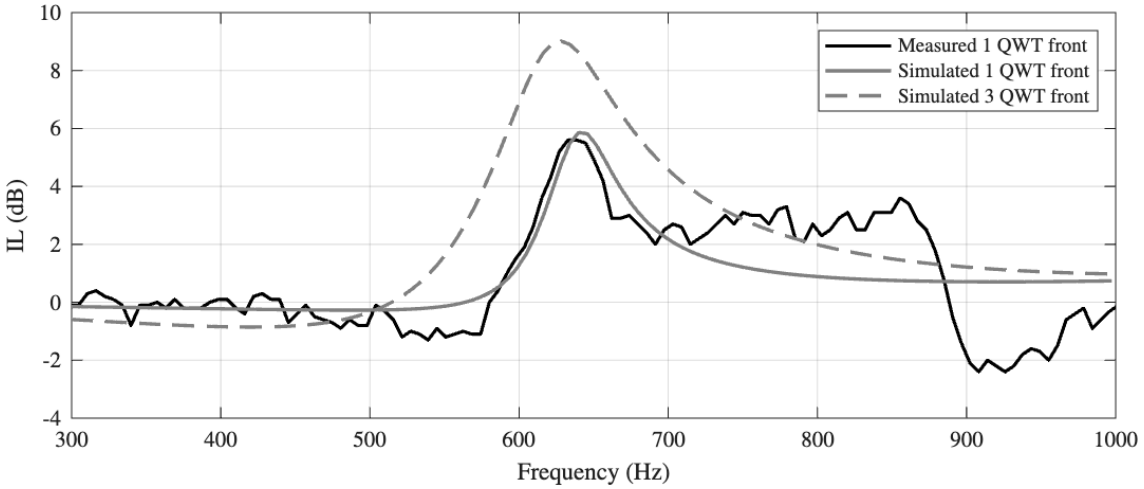


Figure 4.13: Measured IL for one front mounted QWT with simulated IL for one and three front mounted QWT including damping in simulation model.

With the tuned simulation model, a new simulation was done, housing three QWT in the front. Figure 4.13 shows the results from the new simulation along with the measured result for one QWT in the front and its corresponding simulation. The new simulation shows that having three QWT mounted in the front would give an IL value of 9 dB. Comparing this to the result in figure 4.8, it's shown that mounting three QWT in the front gives as good attenuation as eight QWT mounted in the back.

5

Discussion

5.1 Including engine body simulations

To obtain predictions from the simulations that are as accurate as possible, the body through which the signal propagates should be included in the model. This means that if the signal travels through the engine body or cone before entering the intake duct and is measured at the outlet, the complete system geometry should be considered. The improvement obtained by including the body through which the signal propagated through was observed in Section 4.1, specifically in the alignment between the measured and simulated IL for the muffler configurations. When including the geometry of the cone body, the attenuation amplitude increased, while the frequency range over which the muffler attenuated decreased.

This behavior could be explained by the fact that the muffler performance is highly dependent on the acoustic impedance and boundary conditions of the connected system. The cone or the crankcase and surrounding engine geometry act as an additional acoustic volume and compliance, which alter the standing wave patterns and resonance behavior within the intake system.

The resonator, however, did not show any noticeable difference in attenuation trend when the engine body was included. Both the attenuation amplitude and the attenuation bandwidth remained nearly unchanged. This can be linked to the resonator behavior being governed primarily by its own local resonance properties, determined mainly by the cavity volume and neck geometry. Unlike the muffler, the resonator functions as an isolated tuned element and is therefore less sensitive to upstream acoustic conditions and global system geometry. As long as the intake duct geometry remained unchanged, the resonator response remained largely unaffected.

This was also one of the reasons why a resonator was chosen for the detailed stage, since the detailed simulations would not require inclusion of the complete engine geometry and could instead be limited to the intake duct. It should also be noted that including more complex geometries requires significantly higher computational time and computational power.

5.2 Amplitude difference between simulations and measurements

When comparing the simulated and measured results, differences can be observed in the predicted attenuation amplitudes. This is primarily because the simulations assume ideal acoustic conditions, including perfectly smooth surfaces, ideal boundary conditions without leakage, ideal excitation, and the absence of atmospheric and material damping. In reality, such conditions cannot be fully achieved experimentally.

Physical effects such as viscous and thermal losses, small leakages at connections, surface roughness, and manufacturing tolerances introduce additional damping into the real system. Furthermore, uncertainties related to intensity probe positioning, excitation repeatability, and environmental conditions may also influence the measured response. As a result, the experimentally measured attenuation generally becomes lower and broader compared to the simulated predictions.

To improve the agreement between simulations and measurements, damping must be introduced into the simulation model, as performed in Section 4.4. However, since there is no exact damping value that can be determined beforehand for the complete system, experimental measurements are still required for calibration of the model. The simulations can therefore provide accurate trend predictions and design guidance, but experimental validation remains necessary to obtain realistic attenuation levels.

5.3 Duct to Resonator Surface Area Ratio

A key parameter governing resonator attenuation performance is the surface area ratio between the resonator opening area and the cross-sectional area of the main duct. This ratio was varied across several of the tuning experiments described in Section 4.3, including changes in resonator placement, number of resonators, and outlet geometry. Table 5.1 summarizes the resulting area ratios for each configuration tested.

Table 5.1: Cross-sectional areas and resonator-to-duct area ratios

Location	**Area [mm^2]**	**Ratio $A_{\mathbf{res}}/A_{\mathbf{duct}}$ [%]**		
		1 resonator.	**4 resonators.**	**8 resonators.**
Resonator	28.3	–	–	–
Front	234.5	12.1	–	–
Middle	178.0	15.9	–	–
Back (coned)	615.0	4.6	–	–
Back (piped)	399.9	7.1	28.3	56.6

As the table shows, placing the resonator closer to the cylinder increases the ratio,

since the intake consists of two separate ducts that merge into one. A resonator mounted at the front therefore couples to a smaller duct cross section, yielding a higher surface area ratio and consequently stronger attenuation. However, this comes with a practical drawback, the higher temperature closer to the cylinder requires a longer resonator to maintain the same resonance frequency, as the speed of sound increases with temperature according to Equation 2.3. This means that while front mounted resonators are acoustically more efficient, they are geometrically more demanding.

The same level of attenuation achieved by a single front mounted resonator can be achieved by increasing either the number of resonators or the resonator opening area at the rear of the duct, both of which increases the duct to resonator surface area ratio. The experimental tuning measurements showed that four rear mounted resonators were needed to match the attenuation of one front mounted resonator at the fundamental frequency. However, both increasing the number of resonators and enlarging the opening radius are constrained by the limited space available beneath the chainsaw hood, making this a less practical solution than it may appear.

The coned outlet geometry introduces an additional reduction in the duct to resonator surface area ratio compared to a straight cylindrical outlet, since the duct cross section is larger at the point where the resonator is attached. This explains the slightly lower attenuation observed for the coned configuration in Figure 4.11, despite the resonator dimensions being otherwise identical.

5.4 Resonator placement and pressure antinodes

The results presented in Section 4.3.1 show that placing the resonator adjacent to the cylinder yields the greatest attenuation at the fundamental tuning frequency of 680 Hz. This finding appears straight forward when considering that the resonator couples to a smaller duct cross section, as discussed in Section 5.3.

However, observing Table 5.1 it appears that the highest ratio is achieved when placing the resonator in the middle of the duct. If duct to resonator surface area was the sole governing parameter, this would be a contradiction, thus another parameter must be at play.

As established in Section 3.2.4, a resonator achieves maximum attenuation when placed at a pressure antinode. It is therefore proposed that the reduced attenuation observed for the middle placement is not a consequence of an unfavorable area ratio, but rather that the middle position does not coincide with a pressure antinode at 680 Hz. This would explain why the middle mounted resonator, despite having a higher surface area ratio, does not outperform the front mounted one.

5.5 Bending the resonator

The bending of the resonator, as shown in the simulations in section 3.4, but also experimentally in section 4.10 showed that bending the QWT does not effect effec-

tiveness in attenuation, rather it introduces a frequency shift. This validated the detailed design proposal model, showing that the ineffective attenuation was not due to bending the resonator.

5.6 Production inefficiencies

The design proposals were prototyped using PLA and SLS 3D printing, which introduced several manufacturing complications. 3D printing typically requires support material to stabilize overhanging features during production. As a result, parts either had to be split into separate pieces and glued together, otherwise residual support material would remain inside enclosed cavities such as the resonator body or the muffler.

For the QWT resonators, removing the internal support material required drilling a hole into the closed end of each tube. This modification may have slightly increased the effective tube length beyond the intended dimension, thereby lowering the resonance frequency relative to the design target.

Additionally, the layer by layer nature of 3D printing produces surfaces with inherent roughness. Since the acoustic simulations assumed perfectly smooth surfaces, this discrepancy introduced additional damping in the physical models that was not captured in the simulated results.

For parts that required splitting and gluing, the integrity of the joints cannot be guaranteed to be perfectly airtight. Any leakage at the bonded interfaces would alter the acoustic boundary conditions within the solutions, potentially reducing its attenuation performance compared to the simulated results.

6

Conclusion

This thesis investigated the reduction of intake noise in a two-stroke chainsaw engine through the design and evaluation of acoustic noise reduction measures. The study focused primarily on the intake system, which is shown to be a dominant noise source when the exhaust is sufficiently silenced. Through theoretical analysis, numerical simulations, and experimental validation, several acoustic concepts were evaluated with the aim of reducing the radiated sound power from the intake without requiring major modifications to the existing chainsaw geometry, keeping the power to weight ratio the same.

The work began with simplified COMSOL models of the intake duct, where quarter-wave tube (QWT) resonators, Helmholtz resonators, hybrid resonators, and muffler configurations were analyzed. The simulations demonstrated that resonator-based solutions are highly effective for narrowband attenuation, particularly at tonal engine orders, while muffler based concepts provide broader attenuation over a wider frequency range. The fourth engine order at 680 Hz was identified as the most critical frequency for intake noise radiation, and therefore became the primary target for the design process.

The simulations further showed that resonator performance is strongly dependent on geometric parameters and placement along the duct. Placement near pressure antinodes yielded the highest transmission loss, while the QWT resonator opening area influenced both attenuation magnitude and bandwidth. Hybrid resonator concepts demonstrated broader attenuation characteristics than conventional HHR and QWT resonators. Muffler configurations with and without porous material produced smoother and broader attenuation curves, but also introduced amplification regions at lower frequencies overlapping with important engine orders.

As the study progressed toward more realistic geometries, the simulations incorporated increasingly detailed representations of the intake system and spatial constraints imposed by the chainsaw chassis. Due to practical limitations in available space and manufacturing feasibility, the QWT resonator was selected as the most suitable final design concept. The resonator solution required relatively minor modifications to the original intake and could be manufactured using 3D-printing methods.

Experimental validation confirmed that the detailed QWT resonator concept did not achieve sufficient attenuation at the target frequency region around 680 Hz.

Although the measured insertion loss fell below simulation predictions, the general trends agreed reasonably well, and attenuation was observed at the odd multiples of the fundamental resonance frequency. However, since the primary focus was on the fundamental resonance, further tuning of the detailed model, both experimentally and in simulation, was carried out to identify the underlying causes and potential improvements.

The tuning showed that changing the placement of the QWT resonator so that it's in a position adjacent to the cylinder yields greater attenuation rather than having it in the back closer to the air filter, which was the initial thought placement. It was also shown that to achieve the same attenuation for one resonator further in the front, four resonators are needed in the back and that bending the resonators did not have an effect on the magnitude of attenuation.

6.1 Future work

The simulations were limited to pressure acoustics and did not account for flow effects, which can alter resonance behavior in a real intake system. Future work should incorporate flow acoustics to provide a more physically complete model, and should also include simulations showing the pressure drops in the intake introduced by the resonator to quantify the effect it has on the engine performance.

Most importantly, the design proposals were never tested under actual engine operating conditions. Full load testing following ISO 22868:2021 is an essential next step to validate performance under realistic temperatures and pressure amplitudes. Future designs should also explore larger resonator opening areas, to reduce the number of resonators needed in the back.

Bibliography

[1] Blair G. Design and Simulation of Two-Stroke Engines. SAE International; 1996.

[2] Forestry and gardening machinery – Noise test code for portable hand-held machines with internal combustion engine – Engineering method (Grade 2 accuracy). Geneva, Switzerland; 2021.

[3] Dittrich M, Carletti E, Spellerberg G. The ODELIA Study on Noise Limits for Outdoor Machinery; 2016. .

[4] Internal combustion Engine-Powered Hand- Held Chain Saws- Safety and Enviromental Requirements. New York, USA: American National Standards Institute, Inc; 2021.

[5] Chain saws. Toronto, CA: Canaidian Standards Assosiation; 2015.

[6] Behrouz C, David S. Intake-port flow behavior in a motored and fired two-stroke research engine. Experimental Thermal and Fluid Science. 1995;(1):86-100. Available from: https://www.sciencedirect.com/science/article/pii/089417779400067I.

[7] Akbar Ali MH, Mohamad Razlan Z, Bakar S, Eswanto E, Maruyama N, Mohamad M, et al. Impact of Intake Manifold Geometry on Power and Torque: A Simulation-Based Study. Journal of Advanced Research in Fluid Mechanics and Thermal Sciences. 2025 03;128:169-80.

[8] Jiaming L. Sound reduction of side-branch resonators: An energy-based theoretical perspective. AIP Advances. 2024. Available from: https://doi.org/10.1063/5.0202598.

[9] Forouharmajd F, Nassiri P, Monazzam MR, Yazdchi M. The estimation of Helmholtz resonator and active noise control to predict noise reduction of fan in an air duct. International Journal of Environmental Health Engineering. 2015;4(1):6.

[10] Catapane G, Petrone G, Robin O, Verdière K. Coiled quarter wavelength resonators for low-frequency sound absorption under plane wave and diffuse acoustic field excitations. Applied Acoustics. 2023;209:109402. Available from: https://www.sciencedirect.com/science/article/pii/

S0003682X23002001.

[11] Howard C, Craig R. Noise Reduction Using a Quarter Wave Tube with Different Orifice Geometries. Applied Acoustics. 2014 02;76:180-6.

[12] Wu C, Chen L, Ni J, Xu J. Modeling and experimental verification of a new muffler based on the theory of quarter-wavelength tube and the Helmholtz muffler. SpringerPlus. 2016 08;5:1366.

[13] Potente D. General Design Principles for an Automotive Muffler. In: Proceedings of Acoustics 2005. Busselton, Western Australia: Australian Acoustical Society; 2005. p. 153-8.

[14] Munjal ML. Acoustics of Ducts and Mufflers. Newark: John Wiley & Sons, Incorporated; 2014.

[15] Eriksson LJ. Higher order mode effects in circular ducts and expansion chambers. The Journal of the Acoustical Society of America. 1980 Aug;68(2):545-50. Available from: https://doi.org/10.1121/1.384768.

[16] Tao Z, Seybert AF. A Review of Current Techniques for Measuring Muffler Transmission Loss. SAE Transactions. 2003;112:2096-100. Available from: http://www.jstor.org/stable/44745590.

[17] Tupov VV. Principles of design for intake noise silencers to meet acoustic and power requirements of two-stroke carburetor engines. AIP Conference Proceedings. 2022;1:040010. Available from: https://doi.org/10.1063/5.0074735.

DEPARTMENT OF ARCHITECTURE AND CIVIL ENGINEERING
CHALMERS UNIVERSITY OF TECHNOLOGY
Gothenburg, Sweden
www.chalmers.se



CHALMERS
UNIVERSITY OF TECHNOLOGY